Basin architecture controls on the chemical evolution and ^{4}He distribution of groundwater in the Paradox Basin

R.L. Tyne[1,2*], P.H. Barry[1], A. Cheng[2], D.J. Hillegonds[2], J-H. Kim[3], J.C. McIntosh[3], C.J. Ballentine[2]

[1] Dept. of Marine Chem. and Geochem., Woods Hole Oceanographic Institution, Woods Hole, MA, USA [2] Dept. of Earth Sci., University of Oxford, Oxford, UK [3] Department of Hydrology and Atmospheric Sciences. University of Arizona, Tucson, AZ, USA.

*Corresponding author: Rebecca.tyne@whoi.edu

For submission to: EPSL

Number of words: Abstract: 297, Main text: 6470 (limit= 6500)

No. of Figures: 6 (+7 supplementary)

No. of Tables: 3 (+ 5 Supplementary)

Keywords: Noble Gases; Helium; Paradox Basin; Crustal Fluid Dating; Groundwater migration

Highlights

- Noble gas isotopes were measured in multiple formations in the Paradox Basin.
- Noble gases are significantly more radiogenic below the Paradox Formation.
- Evidence for meteoric flushing both above and below the Paradox Formation.
- Numerical models show salt can act as a regional barrier to mobile ^{4}He.
- The basement helium flux and lithology are main controls on the diffusive helium flux.

Abstract

Fluids such as ^{4}He, H_2, CO_2 and hydrocarbons accumulate within Earth's crust. Crustal reservoirs also have potential to store anthropogenic waste (e.g., CO_2, spent nuclear fuel). Understanding fluid migration and how this is impacted by basin stratigraphy and evolution is key to exploiting fluid accumulations and identifying viable storage sites. Noble gases are powerful tracers of fluid migration and chemical evolution, as they are inert and only fractionate by physical processes. The distribution of ^{4}He, in particular, is an important tool for understanding diffusion within basins and for groundwater dating. Here, we report noble gas isotope and abundance data from 36 wells across the Paradox Basin, Colorado Plateau, USA, which has abundant hydrocarbon, ^{4}He and CO_2 accumulations. Both groundwater and hydrocarbon samples were collected from 7 stratigraphic units, including within, above and below the Paradox Formation (P.Fm) evaporites. Air-corrected helium isotope ratios (0.0046 - 0.127 R_A) are consistent with radiogenic overprinting of predominantly groundwater-derived noble gases. The highest radiogenic noble gas concentrations are found in formations below the P.Fm Atmosphere-derived noble gas signatures are consistent with meteoric recharge and multi-phase interactions both above and below the P.Fm, with greater groundwater-gas interactions in the shallower formations. Vertical diffusion models used to reconstruct observed groundwater helium concentrations show the P.Fm evaporite layer to be effectively impermeable to helium diffusion and a regional barrier for mobile elements but, similar to other basins, a basement ^{4}He flux is required to accumulate the ^{4}He concentrations observed beneath the P.Fm. The verification that evaporites are regionally impermeable to diffusion, of even the most diffusive elements, is important for sub-salt helium and hydrogen exploration and storage, and a critical parameter in determining ^{4}He-derived mean groundwater ages. This is critical to understanding the role of basin stratigraphy and deformation on fluid flow and gas accumulation.

1. Introduction

The hydrogeology and hydrogeochemistry of sedimentary basins are inherently complex due to their stratigraphic, structural and temporal controls. Therefore it is critical to understand both the present-day and paleo-fluid flow and geochemistry of a basin, which can inform us about lateral and vertical fluid migration, interaction and emplacement. This is important in dating crustal fluids for groundwater resource security, identifying potential CO_2 or nuclear waste disposal sites, and for helium and hydrogen exploration (Torgersen 1980, Hendry et al., 2005; Zhou et al 2006; Cheng et al., 2021).

Noble gases are useful tools for investigating fluid migration within sedimentary basins. The three main terrestrial reservoirs of noble gases (atmosphere, crust, mantle) are isotopically distinct and therefore, the contribution from each to a particular sample can be readily determined (e.g., Ballentine et al., 2002). Noble gas abundance and isotope characteristics have been extensively used to constrain fluid provenance and migration (e.g., Ballentine et al., 1991, 2002; Gilfillan et al., 2008; Barry et al., 2016, 2017, 2018a,b; Byrne et al., 2020). In addition, the distinct noble gas composition of various fluid sources in sedimentary basins have been used to identify and quantify the exchange between different subsurface fluid phases (e.g., Ballentine et al., 2002; Barry et al., 2016, 2018a; Byrne et al., 2020).

Helium, in particular, is an important noble gas as it is not only a valuable resource but can aid in dating crustal fluids. ^{4}He is produced in-situ by the decay of U and Th in aquifer rocks and its concentration is a function of time and aquifer properties. Fluid residence time in sedimentary basin aquifers can be thus evaluated following (Eq. 1; Torgersen 1980):

$$\left[{}^4He\right]_{in-situ} = \frac{\rho J({}^4He)\Lambda\varphi}{\varphi} \times t \quad \text{(Eq. 1)}$$

where ρ is rock density (g/cm^3), φ is porosity and t is groundwater residence time. The parameter Λ defines the efficiency of helium transfer from mineral to groundwater; $J({}^4He)$ is the production rate of ^{4}He in aquifer minerals and is a function of the U and Th concentrations in the rock (Craig and

Lupton, 1976). In practice, ^{4}He accumulation rates in groundwater have large associated uncertainties, since knowledge of these rates depends on uncertain estimates of aquifer rock porosity, density, U/Th content, (diffusive) release rates of ^{4}He from minerals, and aquifer heterogeneity along the integrated flow path of a water parcel in the subsurface (Torgersen, 1980). In addition, many crustal systems have acquired ^{4}He from an external basement ^{4}He flux (e.g., Torgersen and Clarke, 1985; Torgersen, 1989; Cheng et al., 2021). However, calculations of ^{4}He residence times typically assume a constant external flux regardless of lithology and geographic location (e.g., Zhou and Ballentine 2006, Barry et al., 2018a). Understanding the vertical and horizontal fluid migration within a basin can help constrain some of these uncertainties.

The Paradox Basin in the Colorado Plateau has a diverse and dynamic history of paleofluid flow, including widespread hydrocarbon, CO_2 and He migration and accumulation (Figure 1) (Nuccio and Condon, 1996; Gillfilan et al., 2008, 2009, Craddock et al., 2017). The basin is defined by the extent of a kilometer-thick Pennsylvanian evaporite confining unit (Paradox Formation, P.Fm), which has undergone diapirism (Hite and Buckner, 1981; Nuccio and Condon, 1996; Trudgill, 2011, Pederson et al., 2013), and separates the upper and lower basinal aquifer systems. The complex nature of the stratigraphy and fluid flow within the Paradox Basin, makes it an ideal location to investigate communication between hydrostratigraphic units (i.e., basinal aquifer systems) and the role of the basin architecture, including the presence of bedded and diapiric evaporites, on the chemical evolution of groundwater, which will have implications for both He exploration in the basin, waste storage and groundwater dating.

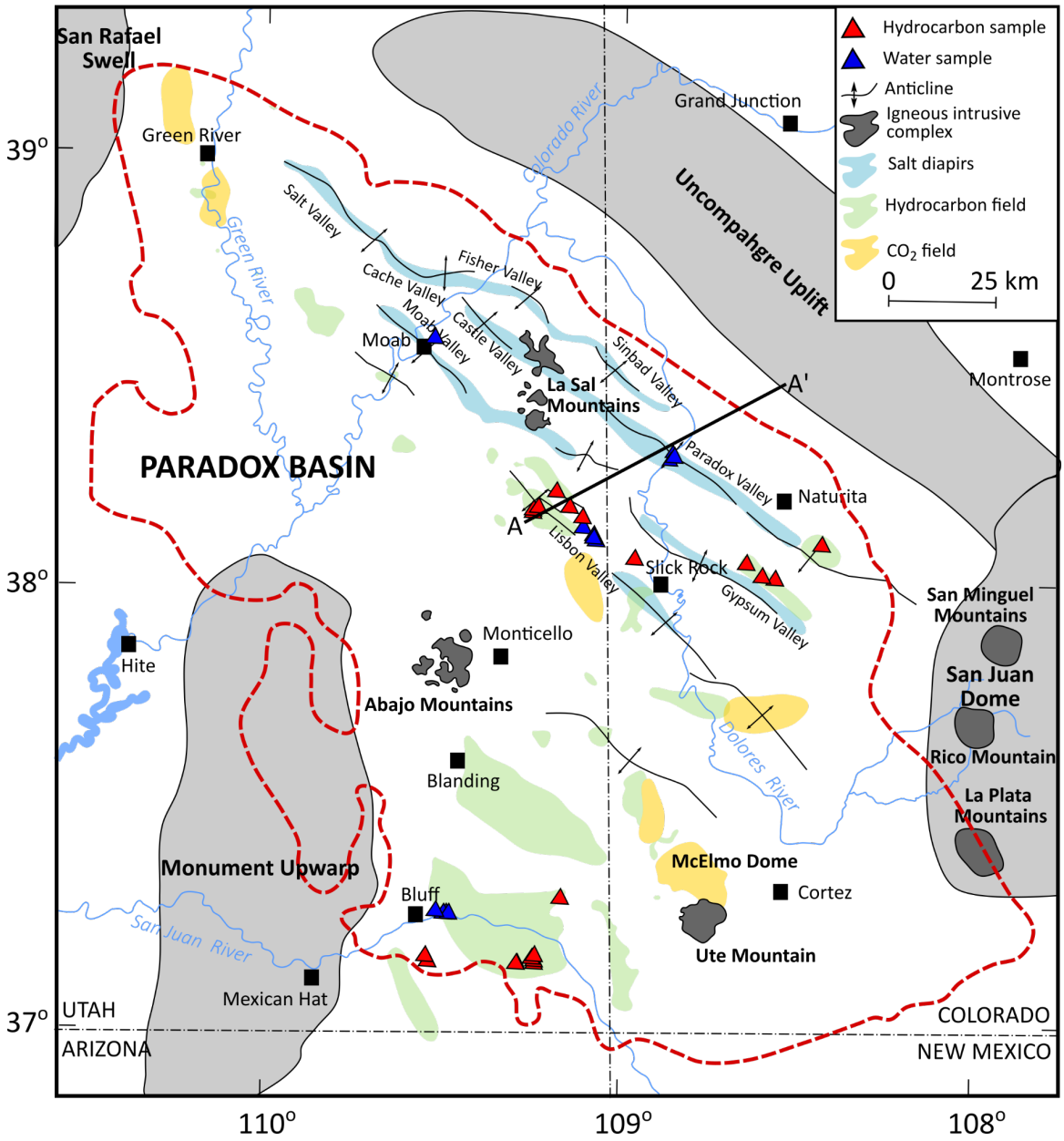

Figure 1: Map of the study area, showing locations of water and hydrocarbon samples taken across the Paradox Basin. The cross section from A-A' can be found in Figure 2. The map has been adapted from Harr (1996) and Kim et al. (2022).

However, to date, there have been no systematic noble gas studies of both the Upper and Lower hydrostratigraphic units across the interior of the basin, despite questions remaining about the patterns and timescales of fluid circulation, migration of mantle derived gases (e.g., CO_2) and potential high He reservoirs (e.g., Dockrill and Shipton 2010, Craddock et al., 2017, Crossey et al., 2006, 2009). In addition, the efficacy of salt as a regional barrier to gas diffusion in areas of faulting

and with extensive salt 'tectonics' has not been investigated and could have significant implication for fluid dating as well as preserving potential exploitable reserves of helium/hydrogen. We present here noble gas isotope and abundance data from samples collected from groundwater and hydrocarbon wells across the Paradox Basin. Samples were taken from throughout the stratigraphic column from both below, within and above the P.Fm (Figure 2) to investigate how the ^{4}He distribution and associated noble gases is affected by the basin architecture (e.g., the widespread occurrence of an evaporite layer) and resulting subsurface fluid regime. Additionally, understanding how the ^{4}He distribution is impacted by an evaporite layer has important implications for understanding basin-scale fluid flow and potential ^{4}He reservoirs.

2. Geological Background and Hydrogeochemistry

The Paradox Basin is an approximately 85,000 km^{2} eastward deepening flexural basin that developed in response to the Late Palaeozoic Uncompahgre Uplift of the ancestral Rocky Mountains (Hanshaw and Hill, 1969; Nuccio and Condon, 1996; Barbeau, 2003). The sedimentary rocks of the Paradox Basin overlie an early Proterozoic basement. A detailed geological history can be found in the SI.1.

There are three hydrostratigraphic units in the Paradox Basin, Upper (Post Paleozoic-Permian formations), Middle (Pennsylvanian P.Fm) and Lower (Devonian-Mississippian formations). The Lower hydrostratigraphic unit (below the P.Fm), containing the hydrocarbon-bearing McCracken Sandstone (Devonian) and Leadville Limestone (Mississippian) (Figure 2), receives local meteoric recharge around the Abajo and La Sal mountains and margins of the salt anticlines (Hanshaw and Hill, 1969; Thackston et al., 1981). It has been hypothesized there is downward fluid flow throughout the basin based on a lower potentiometric surface of the Lower hydrostratigraphic unit compared to the Upper hydrostratigraphic unit, although the Lower unit is less affected by local topography (Hanshaw and Hill, 1969).

The Middle hydrostratigraphic unit (composed of the P.Fm) is a regional confining unit (Thackston et al., 1981; Hanshaw and Hill, 1969). The P.Fm is comprised of 1.8-2.5km thick evaporites

interbedded with dolomite and black shales (e.g., in the Desert Creek and Cane Creeks members), which are important hydrocarbon source rocks (Hite and Buckner, 1981; Nuccio and Condon, 1996; Trudgill, 2011). Following deposition, the P.Fm has undergone sediment loading and passive salt diapirism leading to a series of northwest-southeast trending salt walls and mini basins (e.g., Figure 2) (Trudgill, 2011).

Notable formations to this study in the Upper hydrostratigraphic unit include the Cretaceous Burro Canyon Formation (Fm) (which forms the Burro Canyon Aquifer), Triassic Navajo and Entrada Fms (which form the Navajo Aquifer), Permian Cutler and Pennsylvanian Honaker Trail Fms (Figure 2). During the Tertiary to Holocene (4-10Ma; Lazear et al., 2011; Karlstrom, et al., 2012, Murray et al 2019), present day topographic gradients were formed through erosion of Cretaceous and Cenozoic formations, including the Mancos Shale (Nuccio and Condon, 1996), and incision of the Colorado River and its tributaries. The Laramide Orogeny and emplacement of related laccoliths aided in the creation of the higher topographic gradients. Groundwater flow in the Upper hydrostratigraphic unit (i.e., above the P.Fm) is mainly controlled by topography (Hanshaw and Hill, 1969; Thackson et al., 1981; King et al., 2014). Groundwater flow at the base of this unit directly dissolves evaporites in the underlying P.Fm (Kim et al., 2022).

Although there is no hydrogeological data, flow within the Precambrian basement is likely, given several hairline and open fractures and porosities which can exceed 9% (Bremkamp and Harr, 1988). Moreover, radiogenic strontium ($^{87}Sr/^{86}Sr$ up to 0.735) from basinal fluid circulation through the basement rocks has previously been identified on the Colorado Plateau (Crossey et al., 2006; Kim et al., 2022).

Previous paleofluid studies in the Paradox Basin have focused primarily on the rock record, with inferences about paleofluid origin, composition, flowpaths and mixing (e.g., Beitler et al., 2003; Parry et al., 2004; Dockrill and Shipton 2010). A recent study examined the hydrogeochemistry of fresh to saline formation waters across the hydrostatic units to constrain the fluid sources and geochemical evolution of paleofluids responsible for the sandstone bleaching and associated ore

mineralisation within the Paradox Basin (Kim et al., 2022). They found dilution of connate brines and dissolution of evaporite minerals by meteoric waters in hydrostratigraphic units above and below the P.Fm. This occurred during the past ~3-500ka and >800ka in the lower and upper hydrostratigraphic units, respectively based on ^{14}C and ^{81}Kr dating (Kim et al., 2021, 2022). They suggest recent erosion of the Mancos Shale confining unit and creation of higher topographic gradients, from incision of the Colorado Plateau starting ~10 to 4 Ma (Lazear et al., 2011; Karlstrom et al., 2012, Murray et al., 2019), enhanced deep meteoric water circulation and flushing of connate brines (Kim et al., 2021, 2022). Connate brines, formed from highly evaporated paleoseawater, have been retained within shale interbeds in the P.Fm, likely due to its low permeability, high salinity of fluids, and relatively short time period of meteoric flushing in adjacent aquifer systems (Ferguson et al., 2018; McIntosh and Ferguson, 2021; Kim et al., 2022).

Noble gases have previously been measured in gas fields around the exterior of the Paradox Basin on the Colorado Plateau, as well as at McElmo Dome in the southeast of the basin (Gilfillan et al., 2008; Craddock et al., 2017). These fields are either dominated by hydrocarbons, CO_2 or N_2-He-Ar. The N_2-He-Ar rich fields are predominantly derived from crustal radiogenic production and are associated with structures and sutures in the Precambrian basement. The CO_2-rich fields (including McElmo Dome) have CO_2 concentrations >75% and are magmatic in origin (Gilfillan et al., 2008; Craddock et al., 2017). Mantle CO_2 and helium have also been observed in CO_2 rich seeps across the Plateau (Crossey et al., 2006, 2009, 2016). Additionally, noble gases were measured in shallow groundwaters (Quaternary Valley Fill Aquifer and Lower Jurassic to Upper Triassic Glen Canyon Aquifer, Upper hydrostratigraphic unit) in the Moab and Spanish Valleys (northern Paradox Basin), to better understand the groundwater system, recharge sources and flow directions (Masbruch et al., 2019).

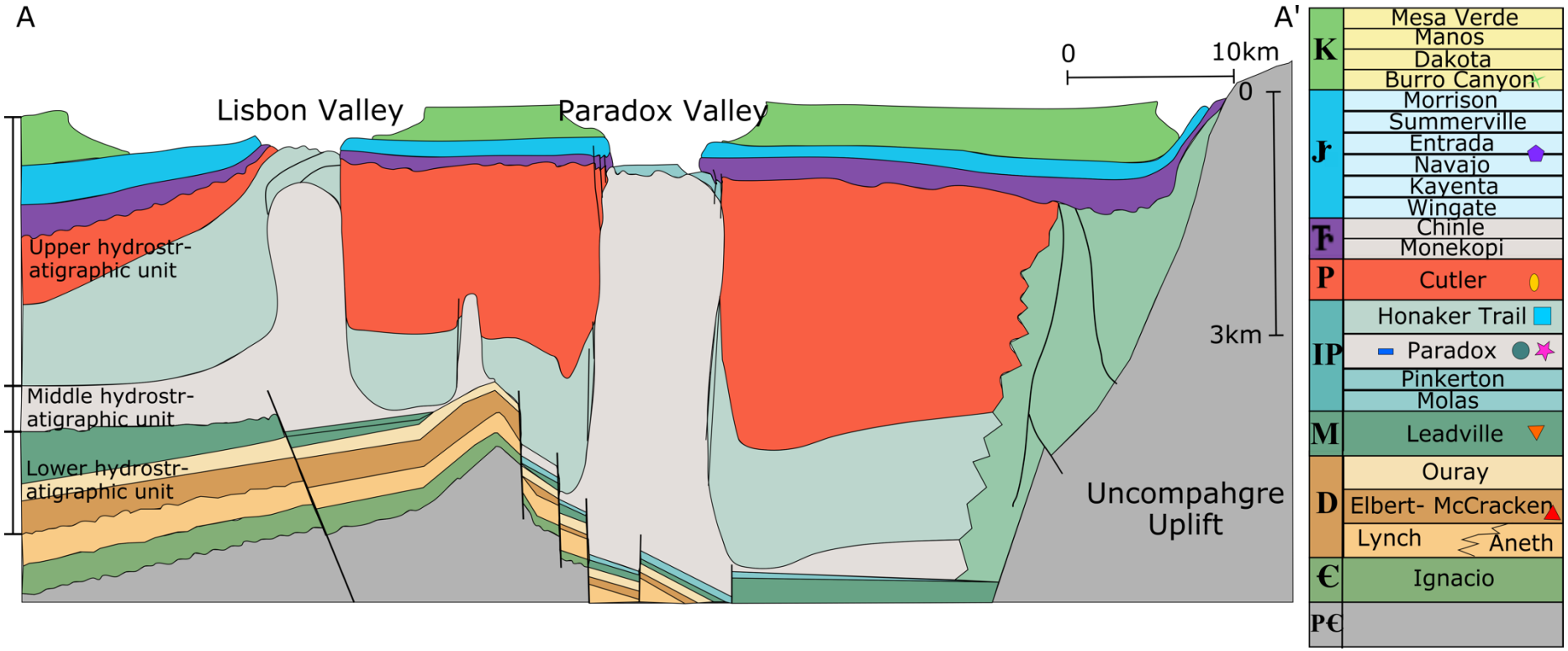

Figure 2: Cross section of across part of the Paradox Basin (A-A', see Figure 1), showing the variation in formation thickness across a subsection of the basin. Modified from Baars and Stevenson (1982), Baars (1996), King et al. (2014) and Kim et al. (2022). A simplified stratigraphic column for the Basin can be found to the right of the cross section (modified from Nuccio and Condon (1996)). Colours used within the cross section correspond to those in the stratigraphic column, and sampled formations are marked with symbols (used hereafter).

3. Methods

A total of 48 samples including 12 duplicates were taken from across 7 stratigraphic units in the Paradox Basin (Figure 2, Table 1, Supplementary Table 1). Shallow groundwaters (n=15) were collected from the Paradox Valley, Lisbon Valley and Greater Aneth Oil Field and 1 deep brine was collected from an artesian lithium exploration well in the Cane Creek member of the P.Fm. The groundwater samples from the Paradox Valley (Salt Diapir) are shallow brines (~14m depth), formed by salt dissolution from meteoric circulation at the top of a salt wall, collected from brine extraction wells adjacent to the Dolores River. The remaining samples (11 produced gases, 8 casing gases (gases that exsolve and migrate up the well casing during production) and 1 produced fluid (condensate, water, gas mixture)) were taken from oil and gas fields across the basin (Figure 1).

Water and produced fluid samples were collected in 3/8" refrigeration-grade copper tubes with stainless steel clamps following the methods described in Tyne et al. (2019). Casing gases were collected in Cu tubes using standard sampling methods (e.g., Barry et al., 2016). Noble gases were analysed in the Noble Laboratory at the University of Oxford, where there is a dedicated offline fluid extraction system, hydrocarbon extraction system and a purification line interfaced to two noble gas mass spectrometers. Full analytical procedures can be found in Tyne et al. (2019).

4. Results

All noble gas concentrations, isotope ratios and associated 1σ errors are reported in Tables 1 and 2. Noble gas concentrations in the gas phase of produced fluids and casing gases have been shown to yield similar information about the subsurface system (Tyne et al., 2021). Therefore, for the produced fluid sample (MC 17-21), the concentration in the gas phase has been calculated following the methods in Tyne et al. (2019), assuming the different phases are at equilibrium, and hereafter is treated as a 'gas' phase sample. Due to solubility within elements being approximately the same for all isotopes, differences in the noble gas isotope ratios between the phases are expected to be negligible and therefore, the overall produced fluid, groundwater and gas phase ratios are directly comparable.

4.1 Helium

Measured helium isotopes ($^3He/^4He$) are between 0.005 and 0.79 R_A where R_A is the atmospheric ratio (R_A=1.4x10^{-6}). Assuming all ^{20}Ne is atmosphere derived, the $^4He/^{20}Ne$ measured in the sample relative to the air value (0.32) for gas phase samples or air saturated water (ASW) (0.25 at 10°C, 0M, 2000m) for water phase samples can be used to calculate the atmospheric He contribution, which is then subtracted from the measured $^3He/^4He$ (Hilton, 1996). When the $^4He/^{20}Ne$ is high, the correction is negligible, however it can be significant when the measured $^4He/^{20}Ne$ is close to air/ASW. Measured $^4He/^{20}Ne$ in the samples range from 2.95x10^{-1} to 1.71x10^5 and increase with depth with the shallowest samples having $^4He/^{20}Ne$ closest to air/ASW (Supplementary Figure 1). Where measured $^4He/^{20}Ne$ are within error of the air/ASW, no correction is possible and we assume that all sample helium is atmosphere-derived. Air-corrected helium isotopes ratios in the Paradox Basin range from 0.005 to 0.127R_A (Figure 3). Low $^3He/^4He$ are consistent with the majority of helium being derived from crustal radiogenic production.

Measured helium (^4He) concentrations are between 0.044 and 213 x 10^{-6} cm^3(STP)/g_{water} in the water phase samples and between 195 to 9,210 x10^{-6} cm^3(STP)/cm^3 in the gas phase samples.

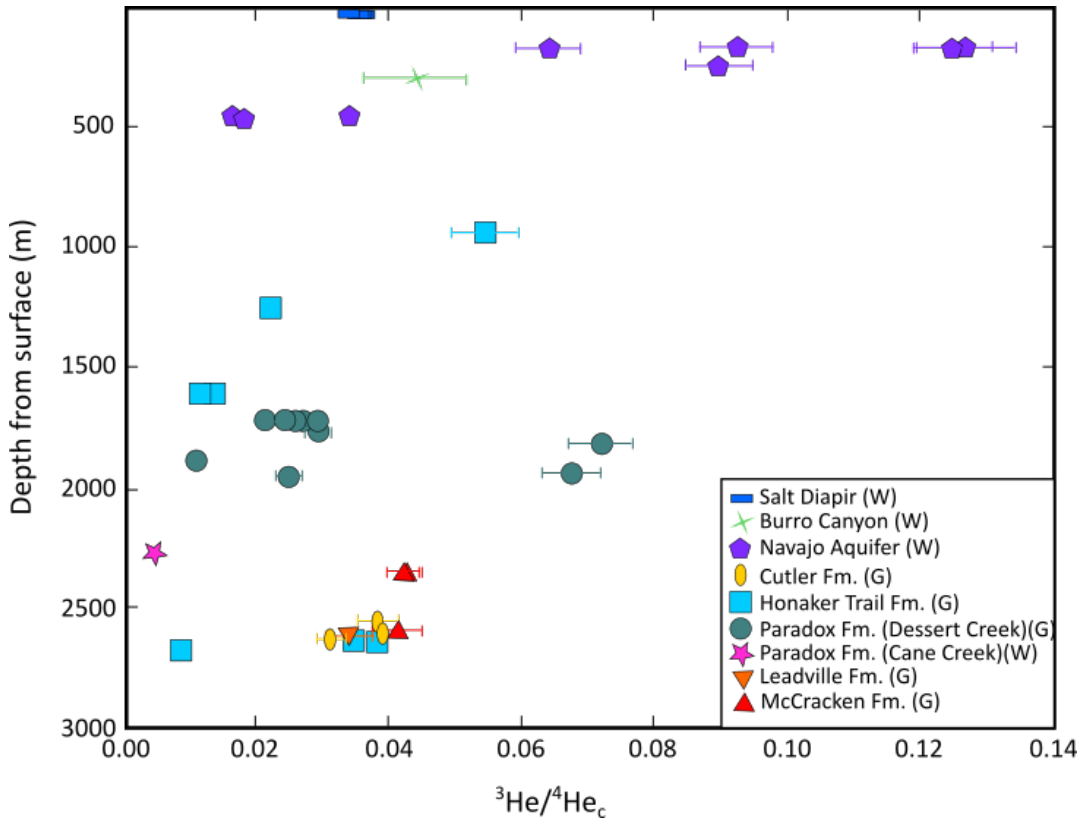

Figure 3: Air Corrected $^{3}He/^{4}He$ (R_c/R_A) as a function of depth from the surface (m). G (gas) and W (water) represent the sample phase. Samples all have low $^{3}He/^{4}He$ relative to sub continental lithospheric mantle (SCLM; 6.1±2.1R_A, Day et al., 2015) and are close to the typical radiogenic production value of 0.02R_A (Ballentine & Burnard, 2002). Elevated $^{3}He/^{4}He$ in the Navajo aquifer are either the result of lower U and Th concentrations in the host rock, or the preferential migration of mantle derived He associated with mantle CO_2 (e.g., Crossey et al., 2016, Byrne et al., 2020).

4.2 Neon

Measured ^{20}Ne concentrations range from 0.084 to 10.3 x10^{-7} $cm^3(STP)/g_{water}$ in the water phase samples and from 0.090 to 82.1 x10^{-7} $cm^3(STP)/cm^3$ in the gas phase samples. Most samples have air-like neon isotopes ($^{21}Ne/^{22}Ne$=0.0290, $^{20}Ne/^{22}Ne$=9.80; Porcelli et al., 2002; Figure 4). Deviations from air are a result of an excess in radiogenically produced ^{21}Ne and ^{22}Ne relative to air or due to mass fractionation effects (Young et al., 2002).

4.3 Argon, Krypton and Xenon

Argon isotope ratios ($^{40}Ar/^{36}Ar$) range from 295 to 4,530. Apart from samples in the Navajo and Burro Canyon aquifers, there is excess radiogenic ^{40}Ar ($^{40}Ar^{*}$) relative to the air value (298.6, Lee et al., 2006). The amount of $^{40}Ar^{*}$ relative to ^{36}Ar is correlated with increasing $^{21}Ne/^{22}Ne$ (Figure 4b). The $^{38}Ar/^{36}Ar$ ratios are between 0.139 and 0.224 and there is no correlation between $^{38}Ar/^{36}Ar$ and $^{20}Ne/^{22}Ne$. Argon abundance (^{36}Ar) ranges from 0.027 to 3.28 x10^{-6} $cm^3(STP)/g_{water}$ in the water phase samples and from 0.025 to 5.5 x10^{-6} $cm^3(STP)/cm^3$ in the gas phase samples.

Krypton (^{84}Kr) concentrations within the gas phase samples range from 0.32 to 7.38 x10^{-8} $cm^3(STP)/cm^3$ and from 0.101 to 9.53 x10^{-8} $cm^3(STP)/g_{water}$ in the water phase. Xenon (^{130}Xe) concentrations are between 0.48 to 386 x10^{-10} $cm^3(STP)/cm^3$ and 0.12 to 5.68 x10^{-10} $cm^3(STP)/g_{water}$ for the gas and water phase samples, respectively. The Kr and Xe isotope ratios are indistinguishable from air in all samples.

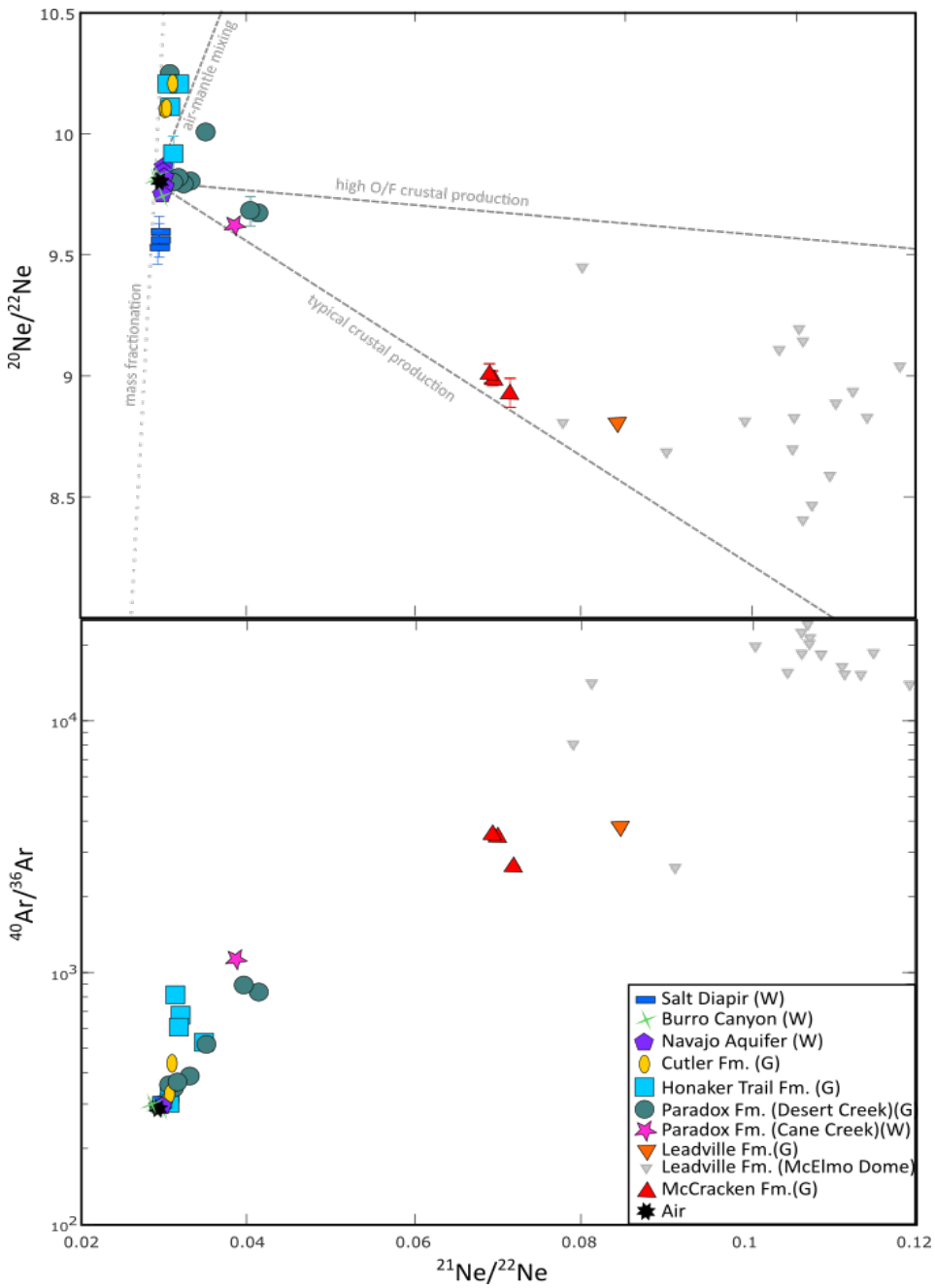

Figure 4: $^{21}Ne/^{22}Ne$ vs. a) $^{20}Ne/^{22}Ne$ and b) $^{40}Ar/^{36}Ar$ for all samples. G (gas) and W (water) represent the phase the sample was collected in. In the formations above the Paradox Formation (Burro Canyon, Navajo, Cutler and Honaker trail) radiogenic noble gases are largely air-like for neon or have relatively small radiogenic Ar excesses. In contrast, the Leadville and McCracken formations beneath the Paradox Formation contain significantly greater proportions of radiogenic noble gases and are consistent with those measured in McElmo Dome (Gilfillan et al., 2008), suggesting the two hydrological systems are disparate. Within the Paradox Formation, neon isotopes show evidence of both typical Oxygen/Florine (O/F) crust in the Cane Creek region and high O/F environments in the Dessert Creek member.

5. Discussion

In the following section we investigate the distribution of noble gases across the Paradox Basin to determine how basin architecture has influenced fluid migration pathways, which is key for both exploration and storage of CO_2, H_2 and nuclear waste. Our approach is to first determine the different fluid sources and their distribution throughout the basin (section 5.1 and 5.2). This gives a first order approximation of if there are any barriers to fluid flow in the basin. We use the fractionation in air derived noble gas ratios to estimate the extent of fluid interaction and migration, and correct noble gas concentrations (section 5.3). Finally, using this information, we develop a 1D vertical He diffusion model, to investigate diffusion barriers and flow through the stratigraphy (Section 5.4).

5.1 Assessing fluid provenance using noble gas isotope ratios

In order to investigate the distribution of noble gases across the basin, it is important to first understand their provenance. Terrestrial noble gas reservoirs (atmosphere, crust and mantle) have diagnostic isotopic compositions, meaning fluids sourced from each reservoir can be distinguished.

Helium isotopes in ASW are readily overprinted by the release of radiogenic ^{4}He in the subsurface. The air-corrected ^{3}He/^{4}He (R_C/R_A) is the sum of two components: the crust and the mantle. The helium isotope ratio associated with typical crustal radiogenic production is $0.02R_A$ (Ballentine & Burnard, 2002) and sub-continental lithospheric mantle (SCLM) is $6.1\pm2.1R_A$ (Day et al., 2015). Air corrected ^{3}He/^{4}He values (0.005 to $0.127R_A$) are consistent with significant radiogenic contributions (Figure 3). The slightly elevated ^{3}He/^{4}He (up to $0.127R_A$) observed in the Navajo Aquifer to the southwest of the basin could either be a result of lower U and Th concentrations in the host rock, or the preferential migration of mantle derived He associated with mantle CO_2 through the aquifer from the Monument Upwarp, as observed regionally and in other basinal systems (e.g., Crossey et al., 2016, Byrne et al., 2020). No CO_2 concentrations were measured in the Navajo Aquifer, however where CO_2 was measured we observe no relationship with helium (supplementary figure 2), suggesting a lack of mantle CO_2 in the basin interior. The primarily

crustal signatures within these samples are in contrast to those measured in distal CO_2 fields (0.125-3.784R_A) which are mantle derived (Gilfillan et al., 2008).

Neon ($^{21}Ne/^{22}Ne$, $^{20}Ne/^{22}Ne$) and argon ($^{40}Ar/^{36}Ar$) isotopes are consistent with mixing between atmospheric and radiogenic endmembers (Figure 4a). In the formations overlying the P.Fm, neon isotope ratios are air-like and deviations from the atmospheric value, in $^{20}Ne/^{22}Ne$, are consistent with mass fractionation effects (Figure 4). However, significant deviations from the atmospheric Ne isotopic compositions are observed within and below the P.Fm that cannot be attributed to mass fractionation. Within the Desert Creek Member of the P.Fm, neon isotopes are consistent with radiogenic production within a high apparent oxygen/fluorine (O/F) environment (Lippmann-Pipke et al., 2011), whereas samples from the Cane Creek Member of the P.Fm, Leadville Fm and McCracken Fm plot closer to production from an environment with an average crustal O/F composition (Kennedy et al., 1990). The Leadville and McCracken Fms, have the most significant crustal Ne contributions and similar to values previously measured in the Leadville Fm at McElmo Dome in the southeast of the basin (Gilfillan et al., 2008).

Samples from the shallow Burro Canyon and Navajo aquifers have air-like $^{40}Ar/^{36}Ar$ (298 to 300, where $^{40}Ar/^{36}Ar_{air}$=298.6, Lee et al., 2006). The remaining samples have measurable $^{40}Ar^*$ with elevated $^{40}Ar/^{36}Ar$ signatures between 302 and 4,530. The $^{40}Ar/^{36}Ar$ generally increases with increasing stratigraphic age and correlates with ^{21}Ne excesses ($^{21}Ne^*$) (Figure 4, Table 2). The most significant $^{40}Ar/^{36}Ar$ excesses (2,620-4,530) are found beneath the P.Fm in the Leadville and McCracken Fms.

Both Ne and Ar isotopes demonstrate a higher radiogenic isotopic contribution beneath the P.Fm compared to samples collected within and above it. We hypothesise from the noble gas isotope ratios that the P.Fm confining unit is acting as a near complete barrier to vertical gas diffusion within the basin, resulting in the accumulation of radiogenic noble gases beneath the P.Fm and the evolution of distinct fluid compositions above and below it. An exception to this is highly faulted regions in the Colorado Plateau, but outside our study area, which facilitate the upward migration of deep fluids (e.g., Crossey et al., 2006, 2016).

5.2 Radiogenic noble gases concentrations

In order to compare radiogenic noble gas (^{4}He, $^{21}Ne^{*}$ and $^{40}Ar^{*}$) concentrations across the basin, measured hydrocarbon phase concentrations are used to calculate the initial noble gas concentration in the associated groundwater (e.g., Cheng et al., 2021; Byrne et al 2020; Barry et al., 2018a, 2018b). Hydrocarbons are assumed to be initially devoid of all noble gases and inherit their atmospheric noble gas signature from solubility exchange with groundwater. The calculated concentrations of ^{20}Ne and ^{36}Ar in ASW are 2.57×10^{-7} cm^3/g_{water} and 1.65×10^{-6} cm^3/g_{water} respectively, based on assumed recharge conditions of 10°C, 0 M, 2000m and a 10% Ne excess (Gilfillan et al., 2008). Noble gases will preferentially partition from the water phase into the gas/oil phase, due to relative solubilities, resulting in a systematically higher proportion of the less water-soluble noble gases in the gas/oil phase and a higher proportion of the more water-soluble noble gases remaining in the water phase (Kharaka and Specht, 1988; Fernàndez-Prini et al., 2003). The extent of this partitioning is moderated by volumes of water to oil/gas. Using the solubility-corrected noble gas ratios and concentrations of atmospheric noble gas in ASW, the concentration of radiogenic noble gases in the groundwater can be calculated from the sampled hydrocarbons (Table 3; SI.2). Concentrations of ^{4}He, $^{21}Ne^{*}$ and $^{40}Ar^{*}$ are correlated and are in agreement with typical crustal production ratios ($^{4}He/^{40}Ar^{*}= 6.01$, $^{21}Ne^{*}/^{40}Ar^{*}= 2.75 \times 10^{-7}$) (Supplementary Figure 4; Ballentine & Burnard 2002), however deviations to higher $^{40}Ar^{*}$ are observed within the P.Fm due to its high ^{40}K content (Hite, 1961).

Groundwater ^{4}He concentration varies by 6 orders of magnitude from 4.40×10^{-8} to 4.40×10^{-2} cm^3/g_{water}. While ^{4}He concentrations are the lowest in the shallowest formations, there is no clear trend with depth below ~1000m (Figure 5a). Salt tectonics have resulted in significant differences in formation thickness across the basin (i.e., Figure 2) and therefore, we compare trends with depth by investigating the concentration vs. stratigraphic age (Figure 5b). There is a clear increase in ^{4}He concentrations with increasing stratigraphic age. The lowest concentrations are in the shallow Burro Canyon Aquifer and the highest concentrations in the deepest McCracken Fm. Calculated in-situ ^{4}He ages (1,750-3,790Ma, Equation 1) are significantly older than stratigraphic ages (~359-382Ma)

below the P.Fm, suggesting an external ^{4}He flux (Table 3). The shallow brines derived from dissolution of halite and gysum in the Salt Diapir (P.Fm) are mostly meteoric and exhibits high sulfide concentrations (5.8-7.1 mmol/L) from bacterial sulphate reduction (Kim et al., 2022) which is being actively exsolved. Both gas stripping from H_2S formation and the meteoric water content accounts for the lower measured ^{4}He concentrations.

A similar trend is also observed in both $^{40}Ar^*$ and $^{21}Ne^*$, with the highest concentrations in the basal Leadville and McCracken Fms below the P.Fm (Supplementary Figure 4), consistent with the strongly nucleogenic $^{21}Ne/^{22}Ne$ and radiogenic $^{40}Ar/^{36}Ar$ ratios observed in these formations. To identify how the P.Fm is controlling the ^{4}He distribution within the basin (Section 5.4), we first need to identify and quantify any fluid interaction (Section 5.3).

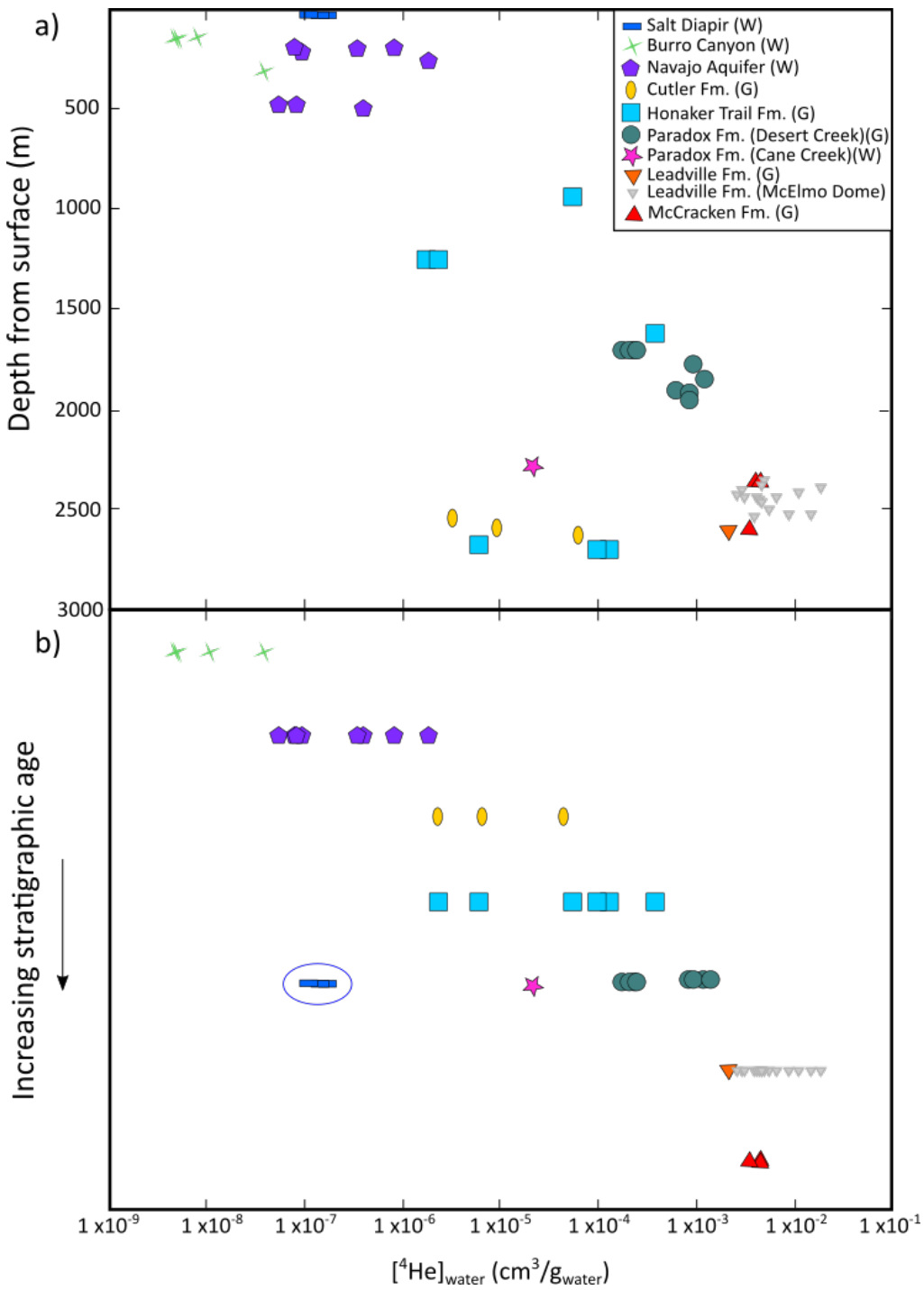

Figure 5: ^{4}He concentration in the water phase vs. a) depth and b) stratigraphic age. G (gas) and W (water) represent the phase the sample phase was collected in. 1 sigma errors are within symbol size. Samples show an increasing ^{4}He concentration with depth/stratigraphic age. McElmo Dome samples are from Gilfillan et al. (2008). Salt Diapir samples (encircled on b) have lower concentrations than the rest of the Paradox Formation, likely due to their shallow, meteoric origin, gas exsolution and adjacent location next to the Dolores River.

5.3 Fractionation of the atmospheric noble gases

Understanding phase fractionation in a system is important for understanding the subsurface environment (e.g., fluid migration, relative volumes) and for correcting concentrations back to original source values. If a system is in equilibrium, the distribution of atmospheric noble gases (^{20}Ne, ^{36}Ar, ^{84}Kr, ^{130}Xe) and ratios ($^{20}Ne/^{36}Ar$, $^{84}Kr/^{36}Ar$, $^{130}Xe/^{36}Ar$) in each phase (e.g., water and gas, water and oil) can be predicted based on their relative solubility. Deviations from these predicted compositions are a result of phase fractionation (SI.4).

Groundwater samples from the Burro Canyon and Navajo aquifers, have $^{20}Ne/^{36}Ar$ within error of ASW (Supplementary Table 2), suggesting little to no fluid interaction/phase fractionation has occurred. Similarly, we see $^{20}Ne/^{36}Ar$ within oil-water equilibrium limits in the Desert Creek Member of the P.Fm hydrocarbon samples that were not subjected to enhanced oil recovery (EOR) techniques, indicating that they represent a closed system phase equilibrium between oil and water (Barry et al., 2018b, Tyne et al., 2021). Where water injection for EOR has occurred in the Dessert Creek member (WM Field), samples have elevated $^{20}Ne/^{36}Ar$, as a result of air incorporation during EOR (Barry et al., 2018b; Tyne et al., 2021).

If groundwater contacts an undersaturated gas phase (e.g., a pocket of CH_4), noble gases will partition into the gas phase (exsolution) resulting a decrease in $^{20}Ne/^{36}Ar$ and increase in $^{84}Kr/^{36}Ar$ (Barry et al., 2016). $^{20}Ne/^{36}Ar$ below ASW (0.049 and 0.069) and $^{84}Kr/^{36}Ar$ above ASW (0.0504-0.0621) are observed in the Salt Diapir (Supplementary Figure 6a,b), consistent with exsolution alongside H_2S into the atmosphere. By modelling exsolution as an open system, we find between 30-44% of the noble gases originally in the groundwater were stripped into a gas phase (Supplementary Figure 6a,b, Supplementary Table 2). Following models by Barry et al (2016) we predict the volume of gas required to exsolve relative to the water volume (G/W) for the Salt Diaper is between 0.028 and 0.042, suggesting that a larger volume of water, than exsolved gas, is required to explain the observed fractionation (SI.4). The groundwater ^{4}He concentration ($[^{4}He]_{gwc}$) can then be corrected for this gas loss using the solubility corrected $^{4}He/^{20}Ne$ and ^{20}Ne expected in ASW (Eq. 2).

$[^4He]_{gwc}=[^{20}Ne]_{ASW} \times {}^4He/^{20}Ne_{SC}$ (Eq. 2)

where $^4He/^{20}Ne_{SC}$ is the solubility corrected (for exsolution or partial redissolution) ratio (Table 3) and $[^{20}Ne]_{ASW}$ is the expected concentration of ^{20}Ne in ASW under recharge conditions (Supplementary Table 3).

Partial redissolution is a two-stage process. During the first stage, noble gases in groundwater are completely exsolved into a gas phase which was initially low in these elements. In the second stage, the noble gases in the gas phase redissolve into groundwater as a result of groundwater flow bringing gas stripped water into contact with the gas phase, or a change in the physical conditions (e.g., increase in pressure). Elevated $^{20}Ne/^{36}Ar$ in the gas samples, in excess of that which can be explained by simple gas-water equilibrium, is observed both above (0.55-0.76, Cutler and Honaker Trail Fms) and below (0.19-0.34, Leadville and McCracken Fms) the P.Fm, consistent with partial redissolution (Supplementary Figure 6c,d). Partial redissolution has previously been observed at McElmo Dome (Gilfillan et al., 2008). Groundwater flow through these units is in agreement with the relatively young (30-800ka) ^{81}Kr and ^{14}C residence times (Kim et al., 2021, 2022; Noyes et al., 2021) and with the major ion and water stable isotope chemistry of the brines, which suggest there has been dissolution of the P.Fm evaporites as a result of influx of meteoric water (Kim et al., 2022). In the Cutler and Honaker Trail Fms (above the P.Fm), the proportion of noble gases that have been partially redissolved is between 87 and 96% (Eq. S9; Supplementary Table 2), which is significantly greater than the proportion redissolved in the Leadville and McCracken Fms (37-78%, Supplementary Figure 6c,d) and suggests greater water-gas interaction in the Upper hydrostratigraphic unit. We also observe much greater water-to-gas (W/G) volumes in the Cutler and Honaker Trail Fms (W/G=38-49) compared to below the P.Fm (W/G=7-24) (Eq. S6-8; Supplementary Table 2), suggesting that the gas phases in the Cutler and Honaker Trail Fms have contacted a relatively greater volume of groundwater than in the Leadville and McCracken Fms below the P.Fm The disconnect between the Upper and Lower hydrostratigraphic units suggests that lateral groundwater transport is more active above the P.Fm and that the P.Fm is a barrier between the two units, in agreement with the radiogenic isotope ratios (Section 5.1). The extent of

partial redissolution can affect the $^{4}He/^{20}Ne$ and therefore the calculated [$^{4}He_{gw}$] for the gas phase samples and any subsequent residence time estimates. By calculating the change in $^{4}He/^{36}Ar$ and $^{20}Ne/^{36}Ar$ with redissolution, we can predict the resulting change in $^{4}He/^{20}Ne$. We find that with 100% redissolution there is a 9.7% increase in the $^{4}He/^{20}Ne$. Below 95% redissolution, the effect of partial redissolution on the $^{4}He/^{20}Ne$ is within error of our samples (<3%). Nevertheless, by quantifying the extent of partial redissolution, we can iteratively correct the $^{4}He/^{20}Ne$ used for calculating [$^{4}He_{gwc}$] (Table 3).

These finding highlights the utility of stable noble gas isotopes in tracing and identifying the differences in hydrogeological regimes above and below an extensive salt unit, as well as quantifying horizontal fluid migration within a basin that needs to be considered when investigating the ^{4}He distribution.

5.4 Investigating ^{4}He distribution

Helium is the most sensitive noble gas to diffusion due to its high diffusivity in water (Jähne et al., 1987), making it an ideal tracer for investigating diffusional gas transport within a basin. To determine the role of the P.Fm in controlling fluid connectivity and compositions throughout the basin, we can compare the initial ^{4}He distribution in groundwater (i.e., prior to any phase interactions), with predictions from a time-dependent vertical 1D ^{4}He diffusion model (Cheng et al., 2021).

5.4.1 Vertical 1D ^{4}He diffusion reference model

In our reference model we assume there are two sources of ^{4}He within sedimentary units, one from in-situ radiogenic production and another from an external basement flux (Supplementary Figure 7a). We also consider two mechanisms of ^{4}He loss to a unit: meteoric recharge with ASW ('flushing') and diffusion to adjacent formations. We use the simplest scenario, of only in-situ production and vertical diffusion, to create a reference model that predicts the ^{4}He concentrations expected in the groundwater (SI.5) (Cheng et al., 2021). Given the variable thicknesses of the sedimentary units across the basin, discrete models are presented for the different sampling areas. Assumptions about the parameters used in constructing these models (e.g., [U], [Th], porosity, age)

are given in Supplementary Table 4. We assume the effective porosity in the P.Fm is approaching zero (0.00001%) (Beauheim and Roberts, 2002). Notably, U and Th concentrations within the P.Fm are poorly constrained (SI.3).

The ^{4}He concentration in groundwater can then be predicted for the whole sedimentary column, assuming in-situ production and diffusion between lithological units (e.g., grey dashed line Figure 6a,b, Eqs S8-11, SI.5). Models predict that once the P.Fm has reached a thickness of ~50m, ^{4}He concentrations become relatively constant, as diffusion is impeded and concentrations are dominated by in-situ production (Figure 6, Supplementary Figure 7b).

Within the Desert Creek Member of the P.Fm, samples can be split into two subgroups; those with lower ^{4}He concentrations due to EOR in the WM Field ($2.06 \pm 0.61 \times 10^{-3}$ cm^3/g_{water}) and those which have not been subject to EOR ($8.82 \pm 2.13 \times 10^{-3}$ cm^3/g_{water}) (Figure 6a). By comparing the ^{4}He concentrations in the samples in the P.Fm which have not been subjected to EOR to the reference model, we observe that ^{4}He concentrations are remarkably constant over the range of depths sampled and are consistent with those predicted for in-situ production alone. This agrees with the model and demonstrates that the P.Fm is in fact an effective seal, acting as a barrier to ^{4}He diffusion and fluid communication, consistent with the observed noble gas elemental ratios. Although this result is not necessarily surprising, as salt is known to be an effective trap for hydrocarbon migration (e.g., Wescott and Hood, 1994), the verification that salt can act as a regional barrier to mobile elements such as ^{4}He, could have implications for ^{4}He and H_2 accumulations and prospecting. In addition, there are significant considerations for crustal fluid dating, as the assumption of a constant external ^{4}He flux throughout the stratigraphy, used in residence times calculations, is not valid where salt formations are prohibiting diffusion.

^{4}He concentrations in the samples both above and below the P.Fm are not consistent with the reference model (Figure 6a,b). Deviations from the reference models can provide insights into the rates and timings of additional processes (e.g., groundwater circulation, basement flux) occurring within the basin, and allow us to investigate cross formational gas migration.

5.4.2 Identification of lateral advective flow

Samples taken from above the P.Fm (Burro Canyon and Navajo aquifers and the Cutler and Honaker Trail Fms) have ^{4}He concentrations lower than predicted by our reference model (grey dashed line; Figure 6). One mechanism that can lower the ^{4}He concentrations is lateral (advective) flow of meteoric water into a unit. This meteoric 'flushing' through a stratigraphic unit decreases the ^{4}He concentration. We can simulate this as 'on-off' system within the diffusive model: During complete flushing, the ^{4}He concentration is effectively 'reset' to ASW concentrations and once lateral flow ceases, ^{4}He accumulation is restarted. Complete flushing of meteoric water has been added to the ^{4}He diffusional model from the recent denudation of the Colorado Plateau (~6Ma; Lazear et al., 2011; Karlstrom et al., 2012, Murray et al., 2019) to 5ka in the Burro Canyon Aquifer, to 25ka in the Navajo Aquifer (average ^{14}C groundwater residence time; Noyes et al., 2021), and to ~0.5 Ma in the Cutler and Honker Trail Fms based on preliminary ^{81}Kr results (Kim et al., 2021, 2022) (Figure 6c,d). Meteoric recharge in these units accounts for the lower ^{4}He concentrations observed within the samples overlying the P.Fm (Figure 6c,d). This in agreement with the fractionation observed in atmospheric noble gas ratios (Section 5.3), major ion and isotopic composition of the brines (Kim et al., 2022), and radiocarbon ages (Noyes et al., 2021).

Several samples (PW4, PW8, BWC2, BWC3, TRTP) have higher concentrations than predicted by the model, this deviation could result from the variation in groundwater residence time (e.g., 3.3-11 ka in the Burro Canyon Aquifer, Noyes et al., 2021), meaning ^{4}He concentrations in the model are underestimated, from upwelling of deeper fluid through faults or from differences in U and Th concentrations of aquifer minerals.

Despite having ^{4}He concentrations greater than can be explained by in-situ production (Figure 6b), the fractionation in the atmospheric noble gas ratios (Section 5.3), ^{81}Kr residence time (~0.8Ma), water isotopes and major ion composition of the brines suggest that there has also been some meteoric water influx below the P.Fm (Kim et al., 2021, 2022). PHREEQC inverse modelling suggests that 95.8% of the groundwater in the Leadville Limestone is meteoric while 4.2% is remaining paleo-evaporated seawater-derived brines (Kim et al., 2022). Therefore, we also model

meteoric flushing from 6 – 0.8Ma in the Pinkerton, Molas, Leadville, Ouray and McCracken Fms beneath the P.Fm but include incomplete flushing with 4.2% 'old' ^{4}He rich groundwaters remaining.

5.4.3 Determining the basement helium flux

Regardless of whether there is meteoric flushing below the P.Fm, ^{4}He concentrations in the Leadville and McCracken Fms are higher than can be explained solely by in-situ production and a basement flux of ^{4}He is required (grey dashed reference line and blue line Figure 6b,d). A volatile flux from the Precambrian basement is in agreement with previous observations of radiogenic Sr in the brines below the P.Fm (Crossey et al., 2006, 2016; Kim et al., 2022). Assuming lateral flow through these units from 6-0.8Ma (approximate ^{81}Kr residence time, Kim et al., 2020, 2021) and incomplete flushing with 4.2% 'old' water (enriched in ^{4}He) remaining (Kim et al., 2022), we find a constant basement flux of between 14.5 – 70 x10^{-6} mol ^{4}He/m^{2}/yr (purple and orange lines respectively, Figure 6d) is required to fit the model to the measured ^{4}He concentrations in these units. This is significantly greater than the average basement flux (1.47 x 10^{-6} mol ^{4}He/m^{2}/yr, yellow line Figure 6d; Torgersen and Clarke, 1985).

Elevated ^{4}He fluxes similar to that predicted by the model are observed in volcanic areas and areas under tectonic strain (Torgersen, 2010). However, the intrusion of the proximal La Sal mountains occurred approximately 20 – 31 Ma (Rønnevik et al., 2017), and the associated heat pulse is thought to be short-lived (Getz, 2020). Alternatively, if a larger portion of fluid enriched in ^{4}He is trapped during flushing, a smaller basement flux will be required. It is important to note here that none of these scenarios are mutually exclusive and a combination of them is possible. Additionally, if flushing of these units ended prior to 0.8Ma, a lower basement flux would fit the model; however even with no flushing, a basement flux is still required. A basement ^{4}He flux combined with P.Fm diffusional barrier indicates that He could accumulate beneath the salt.

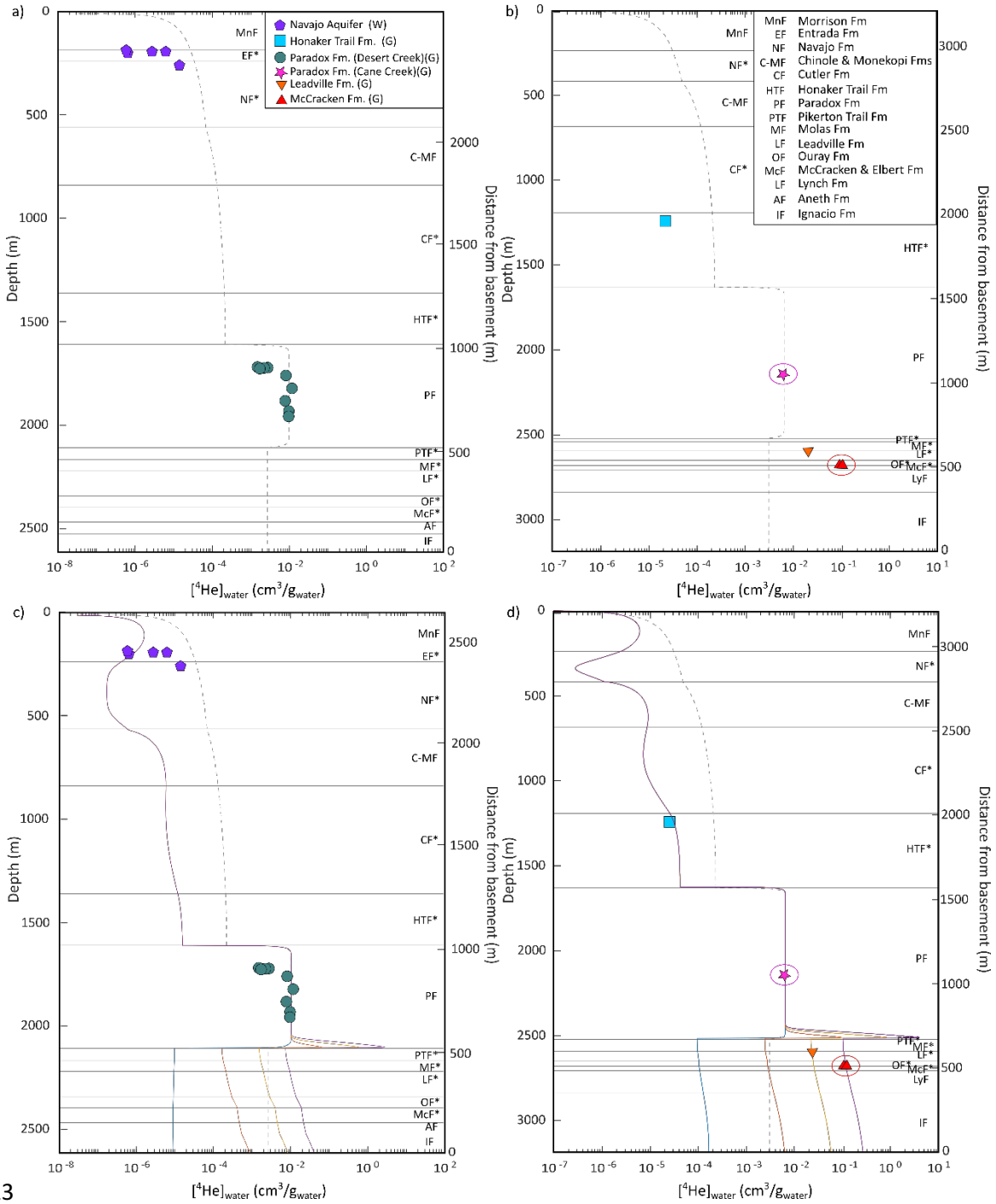

Figure 6: Vertical 1D diffusion model ^{4}He profiles compared with water concentrations inferred for the samples for a) Greater Aneth Oil Field, b) Lisbon Southeast Gas Field, as a function of depth and distance from the Precambrian basement. 1 sigma errors are within symbol size. a) and b) represent the 'reference' model for ^{4}He concentrations in groundwater i.e., in-situ helium production, zero basement flux, no horizontal flow (grey dashed line). McCracken and Paradox (Cane Creek) formations (encircled on b,d) have been transposed from their own discrete models to the appropriate depth and concentration onto profile b/d. ^{4}He diffusion is limited to the bottom ~50m of the Paradox Formation (P.Fm) and the P.Fm samples can be

explained solely by in-situ production. Concentrations lower than predicted by the reference model suggest lateral flushing through these units, where ^{4}He concentrations greater than predicted require a ^{4}He basement flux. c) and d) represent the modelled ^{4}He concentration profiles or groundwater with lateral flow (flushed units marked with *) for different basement fluxes. Modelled basement fluxes (in mol/m^{2}/yr) are as follows: blue=0; yellow=1.5 x10^{-6} (crustal average; Torgersen and Clarke, 1985); purple=14.5 x10^{-6} (required to fit the Leadville Formation sample in the Lisbon Southeast Field); and orange=70 x10^{-6} (required to fit McCracken samples within the Lisbon Field). The convergence of modelled flux lines in the P.Fm is a result of no diffusion within the formation and demonstrates that the P.Fm is effective at preventing vertical communication to the shallower formations.

6. Summary and Conclusions

We present noble gas isotope and abundance data from 36 different samples collected in the Paradox Basin. These samples range across 7 stratigraphic units (Cretaceous-Devonian) and include a thick evaporite unit (Pennsylvanian Paradox Formation, P.Fm). By sampling fluids across a range of stratigraphic units we were able to investigate fluid communication above and below a regional salt layer and between different hydrostratigraphic units within a heterogeneous basin.

Low $^{3}He/^{4}He$ measured across all units is consistent with the noble gases in the system being predominantly groundwater-derived, with radiogenic overprinting. Radiogenic noble gas concentrations (^{4}He, $^{21}Ne^{*}$ and $^{40}Ar^{*}$) and isotope ratios ($^{40}Ar/^{36}Ar$ and $^{21}Ne/^{22}Ne$) increase with depth, consistent with increased accumulation of isotopes formed by crustal production with time, however there is a significant difference in the ratios above and below of the P.Fm as a result of P.Fm acting as a barrier to gas diffusion.

We show that deviations from ASW in atmosphere-derived noble gas ratio ($^{20}Ne/^{36}Ar$, $^{84}Kr/^{36}Ar$ and $^{130}Xe/^{36}Ar$) are a result of phase partitioning during fluid interactions. There is evidence of partial meteoric flushing of remnant basinal brines both below and above the P.Fm, in agreement with the major ion composition of the brines and ^{81}Kr ages (Kim et al., 2020, 2022). Furthermore, we observe greater fluid phase interactions in the samples taken above the P.Fm than below

suggesting that the hydrostratigraphic units above and below the P.Fm are independent, with the upper hydrological regime being more mobile.

Considering both in-situ radiogenic production and external helium basement fluxes, we develop vertical 1D ^{4}He diffusion model. We find that the P.Fm is impermeable to ^{4}He diffusion, allowing for the accumulation of ^{4}He and radiogenic noble gases below. The verification that evaporites are regionally impermeable to diffusion, of even the most volatile elements, is important for sub-salt helium and hydrogen exploration and storage. Deviations from the theoretically calculated ^{4}He diffusion reference model can largely be accounted for by meteoric water recharge, seen in the atmospheric noble gas ratios and likely associated with the recent denudation of the Colorado Plateau. High helium concentrations observed beneath the P.Fm are likely a result of a ^{4}He basement flux and best explained combined with only partial flushing of the units. Typically, the determination of groundwater residence time assumes a simple system of in-situ production and a potential diffusive external flux from below, usually based on an assumed average crustal porosity (Torgersen and Clarke, 1985; Zhou and Ballentine, 2006). Through the development of the ^{4}He diffusional models (e.g. Cheng et al., 2021), we show that the magnitude of the basement flux and lithology type can control the diffusive helium flux. For example, below the P.Fm, where there is a high basement ^{4}He flux and diffusion into shallow formations is inhibited, ^{4}He can accumulate and the ^{4}He residence time would be overestimated. Whereas above the P.Fm, fluid circulation and lack of diffusion from the deepest formations would lead to an underestimation of ^{4}He residence times. Therefore, an understanding and consideration of the basin architecture and history is critical to accurately determine ^{4}He groundwater residence times.

We show that using the stable noble gas isotopes and extent of fluid migration in the basin, the dichotomous hydrostratigraphic units can be identified and the efficacy of the reservoir seal (i.e., P.Fm) can be quantified. This is critical in understanding subterranean modern and paleo-fluid flow within sedimentary basins, such as in the Paradox Basin, as well as for dating crustal fluids. Stratigraphy and regional faulting ultimately controls the connectivity and hydrogeology of various sedimentary reservoirs and understanding the nature and extent of communication between

different fluid reservoirs is critical for resource exploration and storage of alternative energy and anthropogenic waste within the subsurface.

Supplementary figures

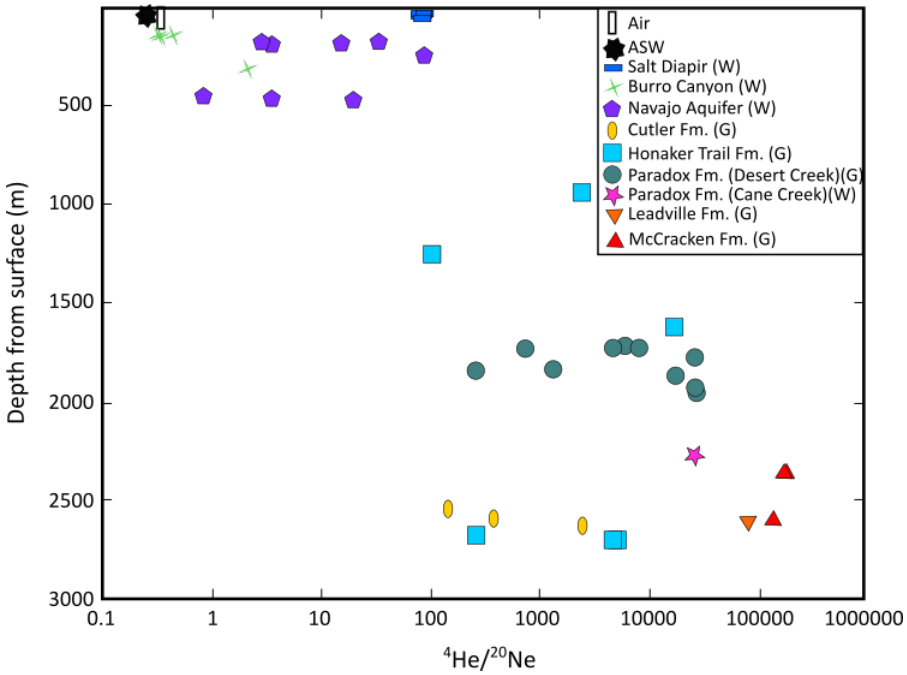

Supplementary Figure 1: $^4He/^{20}Ne$ vs depth across the Paradox Basin. 1σ errors are within symbol size. G (gas) and W (water) represent the sample phase. $^4He/^{20}Ne$ generally increases towards the surface consistent with smaller radiogenic noble gas contributions.

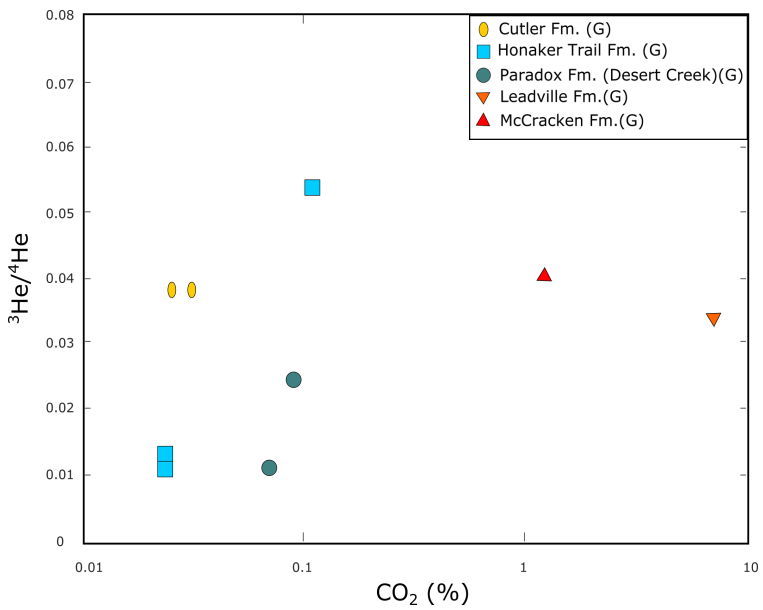

Supplementary Figure 2: Comparison of CO_2 concentration and air corrected helium isotope ratios (Rc/Ra) for gas samples. 1sd errors are within symbol size. There is no relationship between helium isotopes and CO_2 concentrations suggesting a lack of mantle CO_2 in the basin interior.

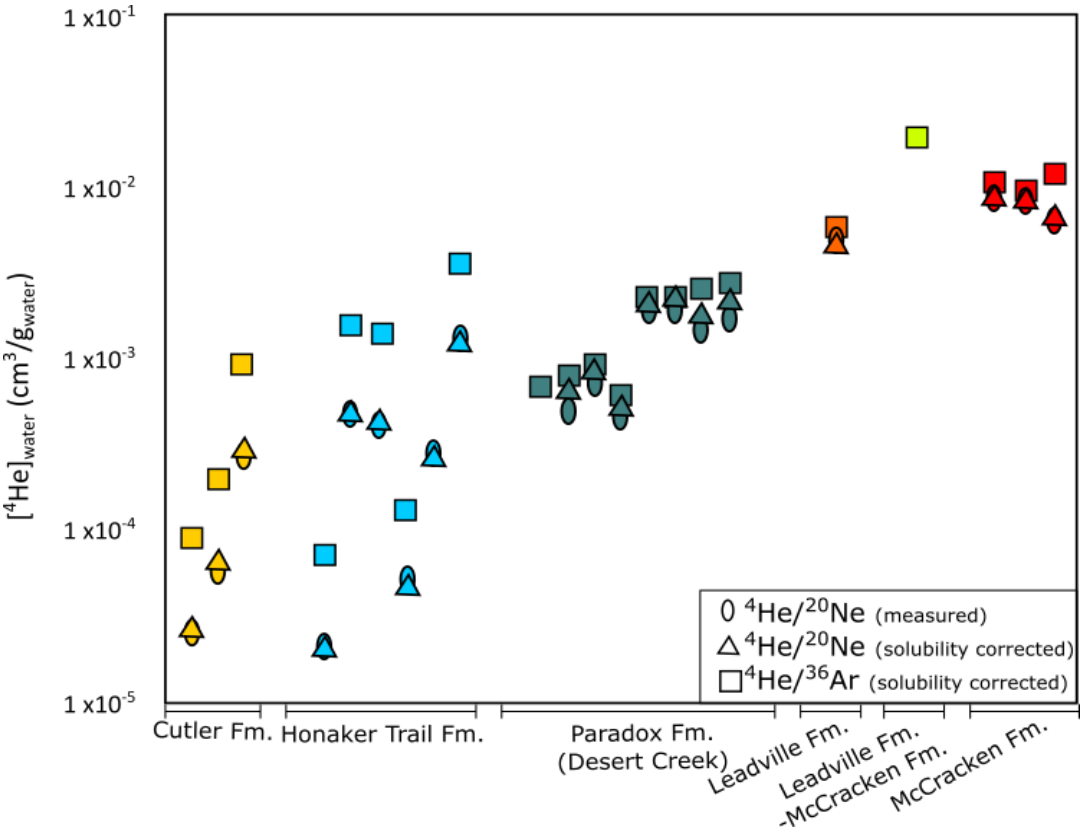

Supplementary Figure 3: Comparison of ^{4}He concentrations in groundwater calculated for the hydrocarbon samples. $[^{4}He]_{gw}$ is calculated using initial atmospheric noble gas concentration in groundwater and the measured $^{4}He/^{20}Ne$ (ovals), the solubility corrected $^{4}He/^{20}Ne$ (triangles) and the solubility corrected $^{4}He/^{36}Ar$ (squares). The Paradox Formation Desert Creek Member samples are from oil fields and have been solubility corrected for oil-water partitioning. The remaining samples are from gas fields and have been corrected for gas-water partitioning. 1 sigma errors are within symbol size. Calculated ^{4}He concentrations from the measured and solubility corrected $^{4}He/^{20}Ne$ are in close agreement, however some variability exists in the 4He concentrations calculated from the solubility corrected $^{4}He/^{36}Ar$, particularly in the Cutler and Honaker Trail formations. The variability from the solubility corrected $^{4}He/^{36}Ar$ concentrations are likely a result of phase partitioning (section 5.3). The ^{4}He concentration from the solubility $^{4}He/^{20}Ne$ has been used to calculate the groundwater ^{4}He concentrations in the text.

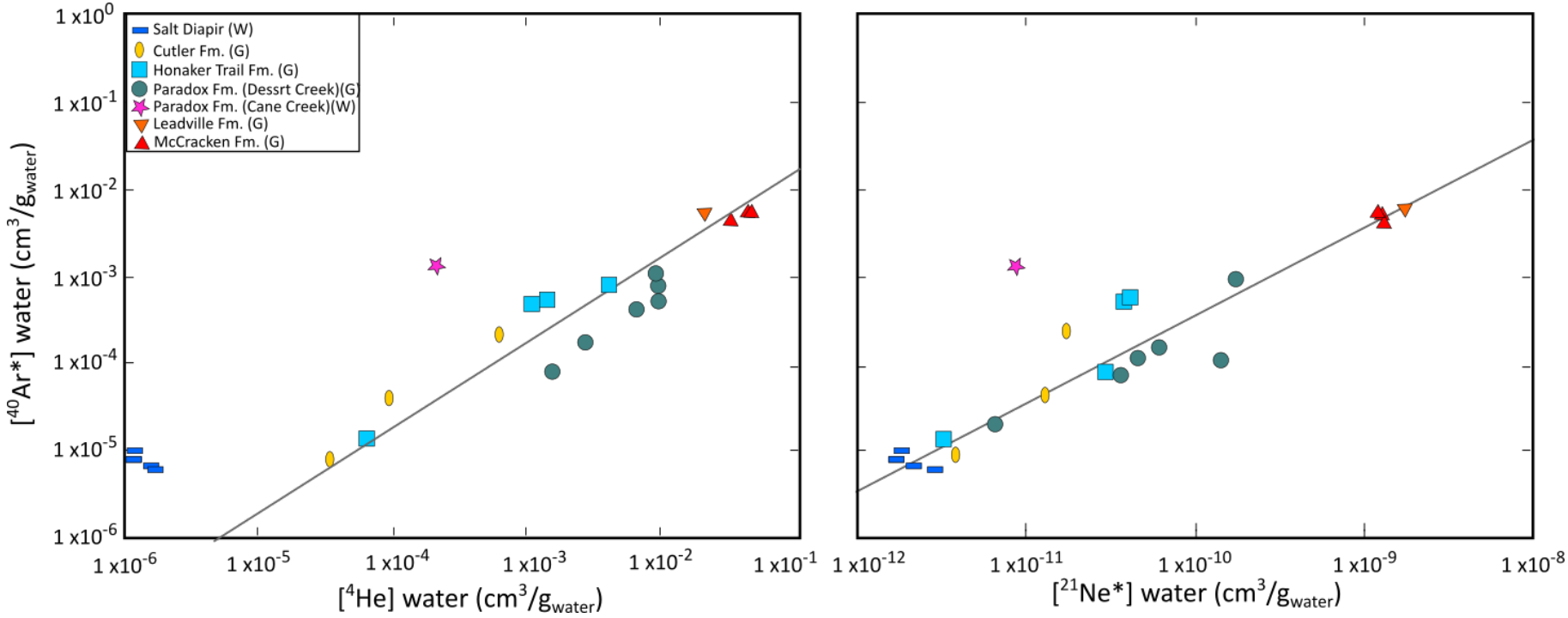

Supplementary Figure 4: Radiogenic isotope abundances in the samples. G (gas) and W (water) represent the sample phase collected. 1 sigma errors are within symbol size. Black lines indicate typical crustal production ratios (see text for details). The majority of samples lie close to typical crustal production, indicating that the bulk radiogenic noble gases have reached the systems without any fractionation (Ballentine et al., 1991). Excess $^{40}Ar^*$ above typical crustal production (relative to ^{4}He and ^{21}Ne) in the Cane Creek Member of the Paradox formation and relative to ^{4}He in the Salt Diapir samples is due to elevated K concentrations (Hite, 1961).

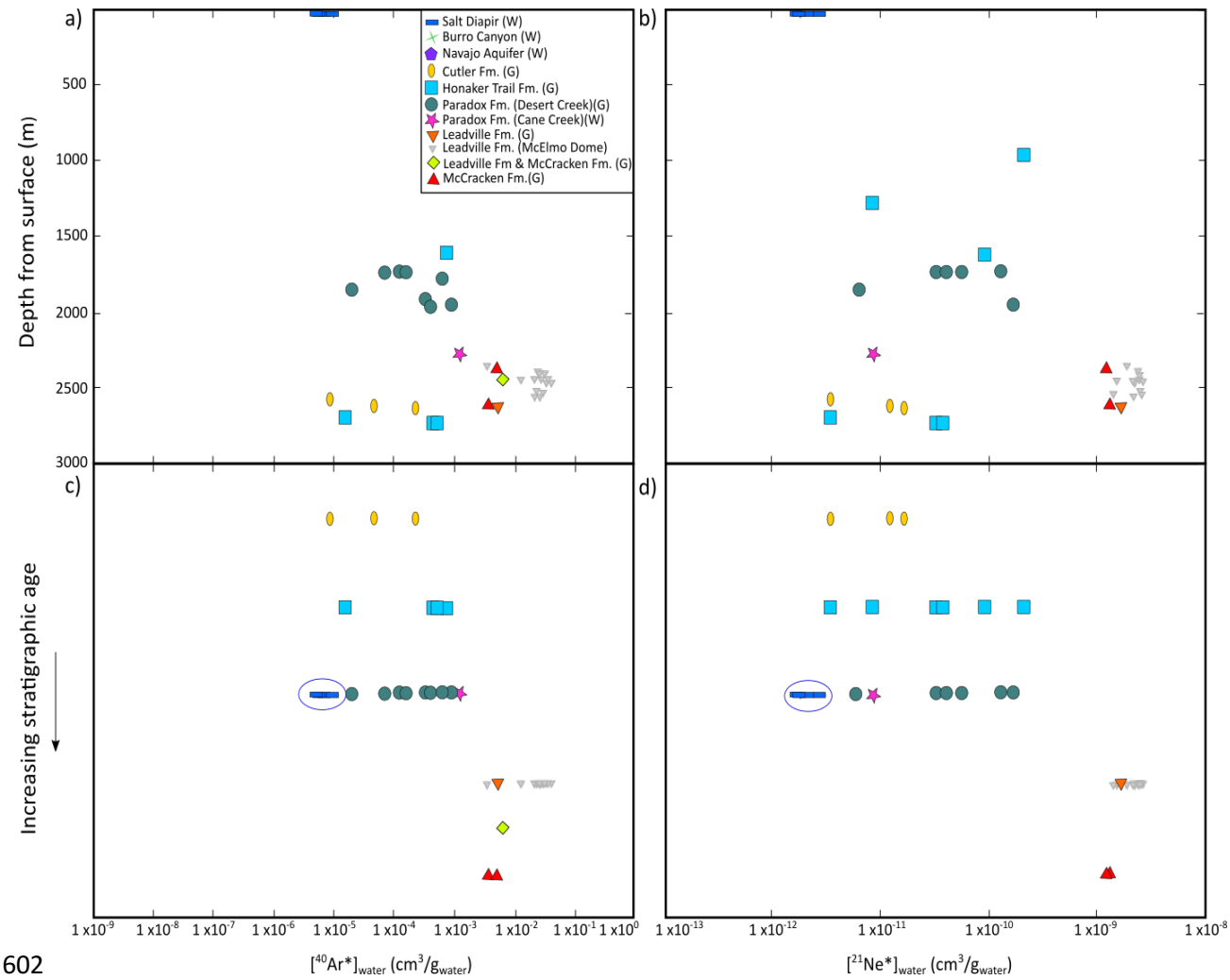

Supplementary Figure 5: Relationship between $^{40}Ar^*$ (a) and $^{21}Ne^*$ (b) with depth. Basin structure means relationships with depth are hard to identify and thus concentration vs. increasing stratigraphic age are also shown (c and d). G (gas) and W (water) represent the sample phase. 1σ errors are within symbol size. a) & c) Samples show increasing $^{40}Ar^*$ accumulation with increasing depth/stratigraphic age with the highest concentrations in the formations beneath the Paradox Formation (P.Fm). b) & d) $^{21}Ne^*$ concentrations within and above the P.Fm are fairly consistent, however a significant increase in $^{21}Ne^*$ is observed below the P.Fm. Salt Diapir samples (encircled) have lower concentrations than the rest of the P.Fm, likely due to their shallow origin, H_2S exsolution and location adjacent to the Dolores River.

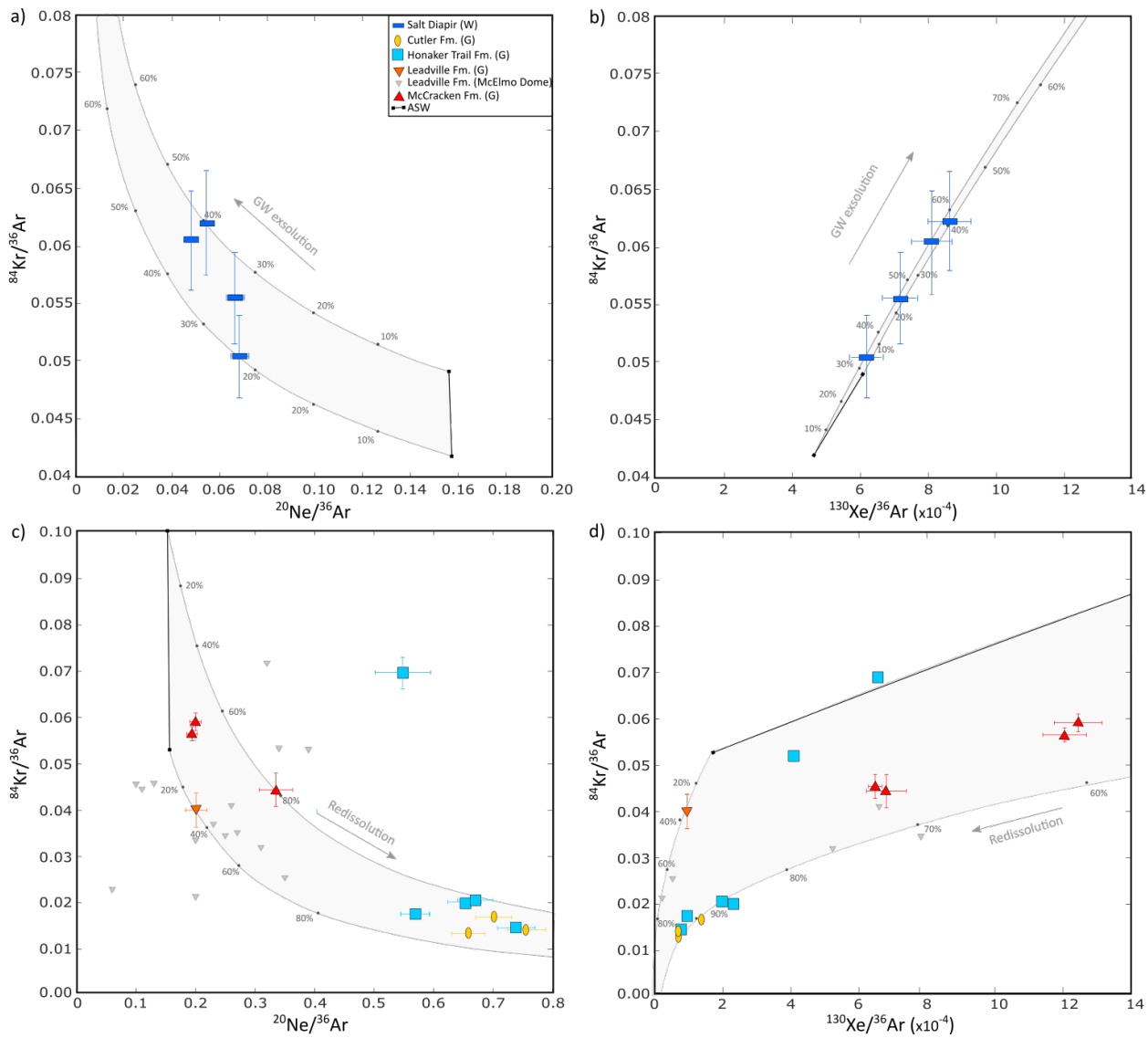

Supplementary Figure 6: Phase (water and gas) fractionation models of exsolution (water to gas; a and b) and partial redissolution (water to gas to water; c and d) for the atmospheric noble gas ratio in the Paradox Basin samples. a) and c) ^{20}Ne/^{36}Ar vs. ^{84}Kr/^{36}Ar. b) and d) ^{130}Xe/^{36}Ar vs. ^{84}Kr/^{36}Ar. a) and b) show groundwater samples alongside the modelled composition of groundwater with exsolution into the gas phase (shaded region). Tick marks represent the percentage of gas exsolved. c) and d) show gas phase samples with the modelled compositions of the gas phase with partial redissolution (shaded region). Tick marks represent the percentage of gas re-dissolved. Partial redissolution of gas into the groundwater accounts for the noble gas data in the McCracken, Leadville, Honaker Trail and Cutler formations, with the greatest proportion of redissolution occurring in the Honaker Trail and Cutler formations. McElmo Dome samples taken from Gilfillan et al. (2008). ASW, in all panels, is modelled for variable Kr and Xe excesses (thick black line, see text).

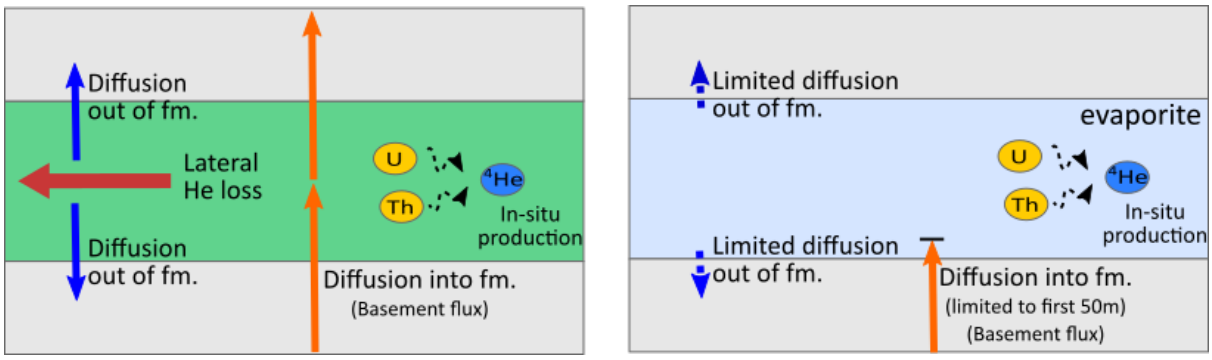

Supplementary Figure 7: Conceptual models for ^{4}He accumulation and loss within a geological formation for (a) the vertical 1D ^{4}He diffusion models and (b) specifically within an evaporite formation. ^{4}He may also result from faulting or mantle contributions however they are not included within the diffusion models. The vertical ^{4}He diffusion models (Figure 9) suggest diffusion into an evaporite formation is limited to the first 50 m and there is only limited diffusion out of an evaporite in comparison to other formations.

Supplementary information

SI.1 Geological Background

Ordivician to mid-Devonian deposits are typically missing at the bottom of the basin due to post Cambrian erosion (Nuccio and Condon, 1996), however notable extant formations relevant to this study are the hydrocarbon bearing McCracken Sandstone (Devonian) and Leadville Limestone (Mississippian) part of the lower hydrostratigraphic unit beneath the Paradox Formation (P.Fm) confining unit (Figure 2).

Large-scale uplift of the Uncompahgre Plateau and subsequent subsidence to the southeast forming a flexural basin (Paradox Basin) defined the Pennsylvanian to Permian period (Nuccio and Condon, 1996; Barbeau, 2003). Fluctuations in sea level controlled sedimentation during the Pennslyvanian period including cyclical desiccation and marine flooding of the basin leading to deposition of the P.Fm, a 1.8-2.5km thick evaporite deposit. The P.Fm is interbedded with dolomite and black shales (e.g., in the Desert Creek and Cane Creeks members) which are important hydrocarbon sources (Hite and Buckner, 1981; Nuccio and Condon, 1996; Trudgill, 2011). Overlying this is the Honaker Trail Fm,

which is composed of cyclically deposited limestone, sandstone and shale (Nuccio and Condon, 1996). The Cutler Fm was subsequently deposited, as a result of the continued uplift, and is comprised of eroded basement rocks (Cater, 1970; Nuccio and Condon, 1996). Simultaneously, sediment loading from the Honaker Trail and Cutler Fms produced a series of northwest-southeast trending salt walls and mini basins through passive salt diapirism (e.g., Figure 2) (Trudgill, 2011).

Triassic to Cretaceous sedimentation of interest includes the red Navajo and Entrada as well as the Burro Canyon Fm. The Navajo and Entrada Fms form the Navajo Aquifer and the Burro Canyon Fm hosts the Burro Canyon Aquifer, these have subsequently been bleached by migration of hydrocarbons, CO_2 or another reducing fluid (e.g., Chan et al., 2000; Beitler et al., 2003; Parry et al., 2004; Dockrill and Shipton 2010; Kim et al., 2022).

During the Tertiary to Holocene (4-10Ma; Lazear et al., 2011, Karlstrom et al., 2012, Murray et al., 2019), present day topographic gradients were formed as a result of erosion of the cretaceous and cenozoic rocks (Nuccio and Condon, 1996) and incision of the Colorado River and tributaries. The Laramide Orogeny and emplacement of laccoliths during this period aided in the creation of the higher topographic gradients.

SI.2 Calculating radiogenic noble gas concentrations in groundwater

Concentrations of radiogenic noble gases in hydrocarbons can be converted to groundwater assuming equilibrium partitioning allowing for the concentrations across the basin to be compared. Hydrocarbons are initially devoid of noble gas signature through interactions with groundwater, as noble gases will preferentially partition into the hydrocarbon phase as a function of their relative solubility. Using the solubility corrected noble gas ratios and concentrations of atmospheric noble gases in ASW (^{20}Ne and ^{36}Ar are 2.57×10^{-7} cm^3/g_{water} and 1.65×10^{-6} cm^3/g_{water} respectively, based on assumed recharge conditions of 10ºC, 0 M, 2000m, 10% Ne excess (Gilfillan et al., 2008)), the concentration of radiogenic noble gases in the groundwater can then be calculated from the sampled hydrocarbons (Zhou and Ballentine, 2006; Cheng et al., 2021).

In previous work the small solubility difference between ^{4}He and ^{20}Ne in groundwater has been neglected, any fractionation assumed to be negligible and the $^{4}He/^{20}Ne$ was assumed to be the same in the different phases (Zhou and Ballentine, 2006; Cheng et al., 2021). Here, we take into account the small differences in solubility between ^{4}He and ^{20}Ne using their solubility coefficients for both gas-water partitioning (Eq. S1) and water-oil partitioning (Eq. S2) (Ballentine et al., 2002).

$$\left(\frac{4He}{20Ne}\right)_{gw} = \left(\frac{4He}{20Ne}\right)_{m} \frac{v_g/v_w + 1/K_w^{He}}{v_g/v_w + 1/K_w^{Ne}} \quad \text{(Eq. S1)}$$

$$\left(\frac{4He}{20Ne}\right)_{gw} = \left(\frac{4He}{20Ne}\right)_{m} \frac{\frac{V_o}{V_w} + \frac{K_o^{He}}{K_w^{He}}}{\frac{V_o}{V_w} + \frac{K_o^{Ne}}{K_w^{Ne}}} \quad \text{(Eq. S2)}$$

where $\left(\frac{4He}{20Ne}\right)_{gw}$ is the $^{4}He/^{20}Ne$ ratio in the groundwater. V_o , V_g and V_w are the volumes of oil, gas and groundwater (estimated from the production data) and K^i_o and K^i_w are the solubilities of noble gas i in oil and water respectively under reservoir conditions (Supplementary Table 3). Notably, changes in reservoir conditions do not have a significant effect on the $^{4}He/^{20}Ne$. The $^{4}He/^{36}Ar$, which can also be used to calculate ^{4}He concentrations, in water phase can be predicted analogously to $^{4}He/^{20}Ne$ using that measured in the hydrocarbon phase (Eq. S1 and S2).

The measured $^{4}He/^{20}Ne$ (neglecting solubility partitioning) and solubility corrected $^{4}He/^{20}Ne$ and $^{4}He/^{36}Ar$ for the water phase can be combined with the ^{20}Ne or ^{36}Ar concentration in ASW, to calculate the expected ^{4}He concentration in the groundwater prior to hydrocarbon interaction ($[^{4}He]_{gw}$)(Eq. S3, Table 3).

$$[4He]_{gw} = [i]_{asw} \times \left(\frac{4He}{i}\right) \quad \text{(Eq. S3)}$$

where i is either ^{20}Ne or ^{36}Ar and the $\left(\frac{4He}{i}\right)$ is either the measured or solubility corrected ratio.

There is good agreement in the calculated groundwater concentrations using the different correction approaches within and below the P.Fm (Supplementary Figure 2). Variance between ^{4}He concentrations

in groundwater calculated using the $^{4}He/^{20}Ne$ and $^{4}He/^{36}Ar$ within the Cutler and Honaker Trail Fms is likely due to open system solubility fractionation (resulting from groundwater flow, see section 5.3) beyond that expected for closed system equilibrium. Given the smaller difference in the solubility between ^{4}He and ^{20}Ne, compared to ^{36}Ar, only the ^{4}He concentration calculated from the solubility corrected $^{4}He/^{20}Ne$, will be considered in the remainder of this study.

Prior to groundwater interaction, hydrocarbon phases contain insignificant amounts of ^{21}Ne and ^{40}Ar (Ballentine et al., 2002). As there is negligible isotopic fractionation associated with the solubility partitioning of noble gases, ^{40}Ar and ^{21}Ne concentrations in groundwater can also be calculated for the gas phase samples using the measured $^{40}Ar/^{36}Ar$ and $^{21}Ne/^{20}Ne$ and predicted ^{36}Ar and ^{20}Ne ASW concentrations (Ballentine et al., 2002). With the exception of McElmo Dome where mantle CO_2 is present (Gilfillan et al., 2008), we assume the Paradox Basin is a two component system consisting of atmospheric noble gas and radiogenic noble gases (Section 5.1). This allows for the radiogenic ^{40}Ar ($^{40}Ar^{*}$) and ^{21}Ne ($^{21}Ne^{*}$) concentrations to be calculated using the following equations (Table 3) (Ballentine et al., 2002):

$$[21Ne^{*}] = [21Ne] \times [1 - (\frac{21Ne/20Ne)_{air}}{(21Ne/20Ne)_{s}}] \text{ (Eq. S4)}$$

$$[40Ar^{*}] = [40Ar] \times [1 - (\frac{40Ar/36Ar)_{air}}{(40Ar/36Ar)_{s}}] \text{ (Eq. S5)}$$

where the subscripts *air* and *s* denote the isotope ratios in air and the samples respectively.

SI.3 ^{4}He residence time

The measured and calculated ^{4}He concentrations in groundwater can be used to calculate the residence time of the water within the system. The ^{4}He residence time for the groundwater assuming solely in-situ production can be calculated/estimated using groundwater ^{4}He concentration, density (assumed to be 2.6 g/cm^{3} throughout), porosity and assuming a 100% release efficiency from the source mineral (Eq.1, Table 3) (Torgersen, 1980; Zhou and Ballentine, 2006).

The concentrations of U and Th within the P.Fm are poorly constrained. The groundwater sample from the Cane Creek Member of the P.Fm is from a lithium exploration well. Li can help facilitate ^{3}He production within the crust and thus a higher $^{3}He/^{4}He$ is expected. Measured Li concentrations in the Cane Creek brine were 110ppm (Kim et al., 2022), however, the measured helium isotopic ratio ($0.0045R_A$) is extremely radiogenic, suggesting that U and Th concentrations within the P.Fm are very low. Using a 0.00001% porosity for the P.Fm (Beauheim and Roberts, 2002), we calculate U and Th concentrations to be 0.18 and 0.69 ppm respectively. We assume slightly higher U and Th concentrations (0.44 and 1.0 ppm respectively) in the Desert Creek Member as the samples are hydrocarbons likely from the carbonate and shale interbeds.

Samples from the Dessert Creek Member of the P.Fm, which have not undergone waterflooding for enhanced oil recovery (EOR), have ^{4}He residences times similar to their formation ages, however both the Cane Creek Member and Salt Diapir samples have lower residence times likely as a result of noble gas partitioning following a change in physical conditions.

For samples where phase interactions were identified (Section 5.3) a 'corrected ^{4}He residence time' accounting for the change in ^{4}He concentrations was calculated (Eq. 2; Table 3).

SI.4 Fractionation of atmospheric noble gas ratios due to fluid interactions

Exsolution

When groundwater contacts an undersaturated gas phase (e.g., a pocket of CH_4), noble gases will partition into the gas phase (exsolution). As Ne is less soluble in water than Ar, a decrease in $^{20}Ne/^{36}Ar$ in the residual groundwater phase occurs together with a proportional increase in the gas phase (Barry et al., 2016). The exsolution of the noble gases in the Salt Diapir is then modelled as an open system(following Rayleigh fractionation) and the proportion of gas that has been exsolved from the Salt Diapir is calculated to be between 30 and 44 % using $^{20}Ne/^{36}Ar$ vs $^{84}Kr/^{36}Ar$ and 18-50% using $^{84}Kr/^{36}Ar$ vs $^{130}Xe/^{36}Ar$ (Supplementary Figure 5a,b, Supplementary Table 2).

The volume of gas required to exsolve relative to the water volume for the Salt Diaper samples can be calculated following equation 12 in Barry et al. (2016). Gas to water ratios between 0.028 and 0.042 are required to cause the observed fractionation, suggesting that a larger volume of water, than exsolved gas, is required to explain the observed fractionation.

Partial redissolution

Partial redissolution causes an increase in the $^{20}Ne/^{36}Ar$ of the gas phase (as ^{36}Ar is more soluble in water) and the initial $^{20}Ne/^{36}Ar$ in the water phase will be low and the ratio will progressively increase to either equilibrium (under closed system conditions) or to higher values (in an open system) and can be modelled following Rayleigh fractionation (Eq. S9):

$$\left(\frac{[i]}{[^{36}Ar]}\right)_{meas} = \left(\frac{[i]}{[^{36}Ar]}\right)_{o} \times f_{\alpha} \quad \text{(Eq.S9)}$$

where i is ^{20}Ne, ^{84}Kr or ^{132}Xe, $[i]/[^{36}Ar]_o$ is the initial atmospheric noble gas ratio in the system, f is the fraction of ^{36}Ar remaining in the gas phase and α is the relative solubility of i and ^{36}Ar. Both the exsolution and the subsequent redissolution of the noble gases are solubility dependent and therefore depend on the relative volumes of gas and water, temperature and salinity of the subsurface environment (Supplementary Table 3). The initial Kr and Xe excesses predicted for each sample are given in Supplementary Table 2. Previous studies (including at McElmo Dome (Gilfillan et al., 2008)) have assumed that the groundwater in stage 2 has been completely degassed (as the groundwater in the initial stage would have been) and the initial gas composition is that of ASW. However, if only small volumes of *partially* degassed water are interacting with the gas phase, the mass balance will result in a negligible change in $[i]/[^{36}Ar]_o$ and thus the predicted trends will be essentially the same.

Elevated $^{20}Ne/^{36}Ar$ in the gas samples, in excess of that which can be explained by simple gas-water equilibrium, is observed both above (0.55-0.76, Cutler and Honaker Trail Fms) and below (0.19-0.34, Leadville and McCracken Fms) the P.Fm, consistent with partial redissolution (Supplementary Figure 5c,d, Supplementary Information S6). Groundwater flow through these units is in agreement with the

relatively young (30-800ka) ^{81}Kr and ^{14}C residence times (Kim et al., 2020, 2021, 2022; Noyes et al., 2021) and with the major ion and water stable isotope chemistry of the brines which suggest there has been dissolution of the P.Fm evaporites as a result of influx of meteoric water (Kim et al., 2022).The influx of meteoric water and flushing of these formations was likely initiated by the denudation to the Colorado Plateau ~4-10Ma (Lazear et al., 2011; Karlstrom et al., 2012, Murray et al., 2019), which removed the Mancos Shale confining unit and created higher topographic gradients (Kim, et al., 2021). The extent of water-gas interaction (i.e., volumetric water/gas ratio, W/G) that has occurred during partial redissolution, can be a useful comparison for the amount of water a gas phase has interacted with. We observed much greater W/G volumes are required in the Cutler and Honaker Trail formations (W/G=38-49) compared to below the P.Fm (W/G=7-24) (Eq. 6-8; Supplementary Table 2) consistent with greater partial redissolution, suggesting that the gas phases in the Cutler and Honaker Trail Fms have contacted a greater volume of groundwater than in the Leadville and McCracken Fms below the P.Fm.

Predicted concentrations for ^{20}Ne and ^{36}Ar in the gas phase are greater than those measured in the gas phase samples, indicating that the noble gases have since been diluted. We define this dilution factor (*D*) as:

$$D = \frac{[i]_{obs}}{[i]_{modelled}} \text{ (Eq. S10)}$$

D = 1 indicates that the observed concentrations are equal to that expected from the models, and a value <1 indicates that dilution has occurred. The calculated dilution factors in the Cutler and Honaker Trail Fms using ^{20}Ne and ^{36}Ar are 0.49±0.25 and 0.48±0.24, respectively. Whereas in the McCraken and Leadville Fms below the P.Fm, *D* values are generally higher (0.78±0.11 for ^{20}Ne and ^{36}Ar) in agreement with the disparity in relative gas-water volumes above and below the P.Fm. This dilution is likely due to groundwater interacting with the hydrocarbon deposits within these units and thus being saturated in terms of methane yet undersaturated in noble gases resulting in the partial redissolution of

noble gases, but not methane. ^{36}Ar concentrations are higher in the Cutler and Honaker Trail Fms than McCracken and Leadville Fms consistent with more groundwater flow through these units.

The brine sample collected from the Cane Creek Member of the P.Fm has similar $^{84}Kr/^{36}Ar$ and $^{130}Xe/^{36}Ar$ values to ASW, however the $^{20}Ne/^{36}Ar$ is elevated (0.31). As only one sample was collected from this formation, no robust model can be developed, however it seems likely that there has been interaction between the brine and another phase and therefore, the initial ^{4}He concentration in the brine prior can be calculated using equation 3 and is 1 order of magnitude greater than measured (3.69 x10^{-3} cm^3/g_{water} compared to 2.13 x10^{-4} cm^3/g_{water}).

The disconnect between the Upper and Lower hydrostratigraphic units suggests that lateral groundwater migration is more active above the P.Fm and that the P.Fm is a barrier between the two units, in agreement with the radiogenic (^{4}He, $^{21}Ne^*$, $^{40}Ar^*$) isotope ratios (Section 5.1). This finding highlights the utility of stable noble gas isotopes in tracing and identifying the differences in hydrogeological regimes above and below an extensive salt unit, as well as quantifying horizontal fluid migration within a basin, that can then be considered when investigating the ^{4}He distribution.

SI.6 Vertical 1D ^{4}He diffusion model

Vertical 1D helium diffusion reference models

Vertical 1D ^{4}He diffusion models were constructed following methods described in Cheng et al., 2021. In the model we assume that each formation is deposited at the beginning of the formation age and has a ^{4}He concentration of ASW (3.04 x10^{-8} cm^3/cm^3). Once deposited, in-situ production (calculated using Eq. 1; Torgersen, 1980) and a flux from depth is initiated. Scenarios were modelled both with and without a ^{4}He basement flux.

The surface was assumed to be equilibrated with air and thus have an ASW composition allowing for diffusive loss. A maximum diffusive flux (J_d) for ^{4}He can be described as in Eq. S11, where diffusion through the unit is a function of time and distance (Eq. S12; Cheng, 2020).

$$J_d = -D_e \frac{\partial C}{\partial Z} \text{ (Eq. S11)}$$

$$\varphi \frac{\partial C}{\partial t} + q \frac{\partial C}{\partial Z} = De \frac{\partial^2 C}{\partial Z^2} + \Phi p \text{ (Eq. S12)}$$

C is the concentration, Z is distance, t is time, φ is rock porosity and p is the production rate per volume (in-situ production). D_e is the effective diffusion coefficient. q is the vertical Darcy's velocity, which is 0, as it is assumed there is no advection. The D_e of ^{4}He in pure water ($D_{e\,He}^{H_2 0}$) is a function of temperature (T, in K) (Ohsumi and Horibe, 1984). A thermal gradient of 30K/km is assumed within the Paradox Basin and the temperature throughout the units is updated on deposition of younger formations.

$$De_{He}^{H_2 0} = 0.02309 e^{\frac{-1706}{T}} \text{ (Eq. S13)}$$

Diffusion within a porous media, as opposed to pure water, will be retarded by both physical and chemical constraints (e.g., grain surface, pore geometry and connectivity). This retardation can be described using a power law model derived by Boving and Grathwohl, 2001:

$$D_e = \Phi^{2.2} D_{e\,He}^{H_2 0} \text{ (Eq. S14)}$$

Within a tight formation D_e is thought to be larger than described in Eq. S14 (Peng et al., 2012). Therefore, within the P.Fm, an effective porosity is used instead of the rock porosity (Shackelford and Moore, 2013).

^{4}He concentrations within the pore spaces of a unit are calculated iteratively with time. A basement flux is added into the deepest formation (in the reference model this is set to 0), the flux into subsequently deposited formations is a function of the ^{4}He concentration in the pore waters directly below. Additionally, the deposition of younger formations at the surface will cause the compaction of underlying formations and a decrease in their porosity, which will increase with time. This decrease in porosity is modelled as a series of steps that occur on the deposition of younger formations and that pore water will be laterally displaced and thus it will not affect the dissolved ^{4}He concentrations in the

pore spaces. We assume the porosity in the P.Fm is not reduced through time due to the nature of a salt layer. Meteoric recharge of ASW ('flushing') was modelling following the methods of Hendry et al., 2015.

Acknowledgements

This work was supported by a Natural Environment Research Council studentship to R.L.Tyne (Grant ref. NE/L002612/1), the W.M. Keck Foundation, and the National Science Foundation (NSF EAR #2120733). J.C. McIntosh and C.J. Ballentine are fellows of the CIFAR Earth4D Subsurface Science and Exploration Program. The authors would like to acknowledge the U.S. Bureau of Reclamation, Paradox Resources, Navajo Petroleum, US Oil and Gas INC, Anson Resources, Lantz Indergard (Lisbon Valley Mining Co.), Ambria Dell'Oro and Mohammad Marza for help with sampling. We also thank David J. Byrne and Rūta Karolytė for their helpful comments on an earlier version of the manuscript, and Grant Ferguson for helpful discussions on Paradox Basin hydrogeology.

References

1. Baars D. L. and Stevenson G. M. (1982) Subtle Stratigraphic Traps in Paleozoic Rocks of Paradox Basin. In: *The Deliberate search for the subtle trap*. AAPG Special Volume. (Ed. Halbouty, M.T.) pp- 131–158.
2. Baars D. L. (1996) Pre-Pennsylvanian Paleotectonics—Key to Basin Evolution and Petroleum Occurrences in Paradox Basin, Utah and Colorado. *AAPG Bulletin* **50**.
3. Ballentine C. J., Burgess R. and Marty B. (2002) Tracing fluid origin, transport and interaction in the crust. In: *Noble Gases in Geochemistry and Cosmochemistry.*(Eds: D. Porcelli, C.J. Ballentine,, R. Wieler) Reviews in Mineralogy and Geochemistry **47**. Geochemical Society, Mineralogical Society of America, Chapter 13, pp. 539–614.
4. Ballentine C. J. and Burnard P. G. (2002) Production, Release and Transport of Noble Gases in the Continental Crust. In: *Noble Gases in Geochemistry and Cosmochemistry.*(Eds: D. Porcelli, C.J. Ballentine,, R. Wieler) Reviews in Mineralogy and Geochemistry **47**. Geochemical Society, Mineralogical Society of America, Chapter 12, 481–538.
5. Ballentine C. J., O'Nions R. K., Oxburgh E. R., Horvath F. and Deak J. (1991) Rare gas constraints on hydrocarbon accumulation, crustal degassing and groundwater flow in the Pannonian Basin. *Earth and Planetary Science Letters* **105**, 229–246.
6. Barbeau D. L. (2003) A flexural model for the Paradox Basin: implications for the tectonics of the Ancestral Rocky Mountains: A flexural model for the Paradox Basin. *Basin Research* **15**, 97–115.
7. Barry P. H., Lawson M., Meurer W. P., Cheng A. and Ballentine C. J. (2018a) Noble Gases in Deepwater Oils of the U.S. Gulf of Mexico. *Geochemistry, Geophysics, Geosystems* **19**, 4218–4235.
8. Barry P.H., Kulongoski J. T., Tyne R. L., Landon M. K., Gillespie J. M., Stephens M. J., Hillegonds D. J., Byrne D. J. and Ballentine C. J. (2018b) Tracing enhanced oil recovery signatures in casing gases from the Lost Hills oil field using noble gases. *Earth and Planetary Science Letters* **496**, 57–67.
9. Barry P. H., Lawson M., Meurer W. P., Warr O., Mabry J. C., Byrne D. J. and Ballentine C. J. (2016) Noble gases solubility models of hydrocarbon charge mechanism in the Sleipner Vest gas field. *Geochimica et Cosmochimica Acta* **194**, 291–309.
10. Beitler, B., Chan, M.A., Parry, W.T. (2003) Bleaching of Jurassic Navajo Sandstone on Colorado Plateau Laramide highs: Evidence of exhumed hydrocarbon supergiants? *Geology* **31**(12) 1041-1044
11. Beauheim, R.L. and Roberts R.M., (2002) Hydrology and hydraulic properties of a bedded evaporite formation. *Journal of Hydrology* **259**(1-4) 66-88.
12. Bremkamp, W., and Harr, C. L. (1988) Area of least resistance to fluid movement and pressure rise: Paradox Valley Unit, Salt Brine Injection Project, Bedrock, Colorado: a report prepared for the U.S. Bureau of Reclamation, Denver, Colorado, 39.
13. Byrne D. J., Barry P. H., Lawson M. and Ballentine C. J. (2020) The use of noble gas isotopes to constrain subsurface fluid flow and hydrocarbon migration in the East Texas Basin. *Geochimica et Cosmochimica Acta* **268**, 186–208.
14. Cheng A., Sherwood Lollar B., Warr O., Ferguson G., Idiz E., Mundle S.O.C., Barry P. H., Byrne D., Mabry J. and Ballentine C. J. (2021) Determining the role of diffusion and basement flux in controlling ^{4}He distribution in sedimentary basin fluids. *Earth and Planetary Science Letters.*
15. Craddock W. H., Blondes M. S., DeVera C. A. and Hunt A. G. (2017) Mantle and crustal gases of the Colorado Plateau: Geochemistry, sources, and migration pathways. *Geochimica et Cosmochimica Acta* **213**, 346–374.

16. Craig H. and Lupton J. E. (1976) Primordial neon, helium, and hydrogen in oceanic basalts. *Earth and Planetary Science Letters* **31**, 369–385.
17. Crossey L. J., Fischer T. P., Patchett P. J., Karlstrom K. E., Hilton D. R., Newell D. L., Huntoon P., Reynolds A. C. and de Leeuw G. A. M. (2006) Dissected hydrologic system at the Grand Canyon: Interaction between deeply derived fluids and plateau aquifer waters in modern springs and travertine.
18. *Geology* **34**, 25–28.
19. Crossey L. J., Karlstrom K. E., Springer A. E., Newell D., Hilton D. R., and Fischer T., (2009) Degassing of mantle-derived CO2 and He from springs in the southern Colorado Plateau region—Neotectonic connections and implications for groundwater systems: *Geological Society of America Bulletin* **121**(7-8) 1034-1053.
20. Crossey, L.J., Karlstrom, K.E., Schmandt, B., Crow, R., Colman*, D., Cron*, B., Takacs-Vesbach, T.D., Dahm, C., Northup, D.E., Hilton, D.R., Ricketts*, J.R., Lowry, A.R., 2016, Continental smokers couple mantle degassing and unique microbiology within continents: Earth and Planetary Science Letters, v. 435, p. 22-30
21. Day, J.M., Barry, P.H., Hilton, D.R., Burgess, R., Pearson, D.G. and Taylor, L.A. (2015). The helium flux from the continents and ubiquity of low-$^3He/^4He$ recycled crust and lithosphere. *Geochimica et Cosmochimica Acta*, 153, 116-133.
22. Dockrill, B., Shipton, Z.K. (2010) Structural controls on leakage from a natural CO_2 geologic storage site: Central Utah, U.S.A. *Journal of Structural Geology* **32**(11) 1768-1782.
23. Ferguson, F., McInotsh, J.C., Grasby, S.E., Hendry, M.J., Jasechko, A., Lindsay, M.B., Luijendijk, E. (2018) The persistence of Brines in Sedimentary Basins. *GRL,* **45**, 4851-4858.
24. Fernández-Prini R., Alvarez J. L. and Harvey A. H. (2003) Henry's Constants and Vapor–Liquid Distribution Constants for Gaseous Solutes in H_2O and D_2O at High Temperatures. *Journal of Physical and Chemical Reference Data* **32**, 903–916.
25. Getz C. M. (2020) Igneous-related hydrothermal systems in a saline basinal setting: La Sal Mountains, Paradox Basin, Utah. Masters Thesis, University of Arizona.
26. Gilfillan S. M. V., Ballentine C. J., Holland G., Blagburn D., Lollar B. S., Stevens S., Schoell M. and Cassidy M. (2008) The noble gas geochemistry of natural CO_2 gas reservoirs from the Colorado Plateau and Rocky Mountain provinces, USA. *Geochimica et Cosmochimica Acta* **72**, 1174–1198.
27. Hanshaw B. B. and Hill G. A. (1969) Geochemistry and hydrodynamics of the Paradox Basin region, Utah, Colorado and New Mexico. *Chemical Geology* **4**, 263–294.
28. Harr C. L. (1996) Paradox Oil and Gas Potential of the Ute Mountain Ute Indian Reservation: Phase II Geology/Seismic Study. *Geology and Resources of the Paradox Basin*, Utah Geological Association, 13–28.
29. Hendry, M.J., Kotzer, T.G., Solomon, D.K., (2005) Sources of radiogenic helium in lcay till aquitard and its use to evaluate the timing of geoligc events. *GCA*, **65**(2), 475-483
30. Hilton, D.R. (1996) The helium and carbon isotope systematics of a continental geothermal system: results from monitoring studies at Long Valley caldera (California, USA). Chemical Geology, 127
31. Hite, R.J., 1961, Potash-bearing evaporite cycles in the salt anticlines of the Paradox basin, Colorado and Utah, in Short papers in the geologic and hydrogeologic sciences: U.S. Geological Survey Professional Paper 424D, p. D135-D138.
32. Hite R. J. and Buckner D. H. (1981) Stratigraphic Correlations, Facies Concepts, and Cyclicity in Pennsylvanian Rocks of the Paradox Basin. In: Geology of the Paradox Basin. Rocky Mountain Association of Geologists 1981 Field Conference
33. Jähne B., Heinz G. and Dietrich W. (1987) Measurement of the diffusion coefficients of sparingly soluble gases in water. *Journal of Geophysical Research: Oceans* **92**, 10767–10776.
34. Karlstrom K.E., Coblentz D., Dueker K., Ouimet W., Kirby E., Van Wijk J., Schmandt B., Kelley S., Lazear G., Crossey, L.J., Crow R., Aslan A., Darling A., Aster R., MacCarthy J.,

Hanse S.M., (2012) Mantle-driven dynamic uplift of the Rocky Mountains and Colorado Plateau and its surface response: Toward a unified hypothesis. *Lithosphere* **4**(1), 3–22

35. Kennedy B. M., Hiyagon H. and Reynolds J. H. (1990) Crustal neon: a striking uniformity. *Earth and Planetary Science Letters* **98**, 277–286.
36. Kim J.-H., Bailey L., Noyes C., Tyne R. L., Ballentine C. J., Person M., Ma L., Barton M. D., Barton I. F., Reiners P., Ferguson G. and McIntosh J. C. (2022) Hydrogeochemical evolution of formation waters responsible for sandstone bleaching and ore mineralization in the Paradox Basin. *GSA Bulletin*.
37. Kim J.-H., Ferguson G.A.G., Person M. A., Jiang W., Lu Z.-T., Yang G.-M., Tyne, R.L., Ballentine C. J., Reiners P. and McIntosh J. C. (2021) Krypton Isotopes Constrain Timing of Regional Meteoric Circulation Enhanced by Rapid Denudation. In *AGU Abstracts*. AGU. New Orleans, LA and Online.
38. King V. M., Block L. V., Yeck W. L., Wood C. K. and Derouin S. A. (2014) Geological structure of the Paradox Valley Region, Colorado, and relationship to seismicity induced by deep well injection. *Journal of Geophysical Research Solid Earth* **119**, 4955–4978.
39. Lazear, G. D., Karlstrom, K. E., Aslan, A., Schmandt, B., Beard, L. S., and CREST Working Group (2011) Denudational flexural isostasy of the Colorado Plateau: Implications for incision rates and tectonic uplift, in Beard, L.S., Karlstrom, K. E., Young, R. A., and Billingsley, G. H., eds., C Revolution 2—Origin and Evolution of the Colorado River System, Workshop Abstracts: U.S. Geological Survey Open-File Report 2011-1210, p. 287-295.
40. Lee J.-Y., Marti K., Severinghaus J. P., Kawamura K., Yoo H.-S., Lee J. B. and Kim J. S. (2006) A redetermination of the isotopic abundances of atmospheric Ar. *Geochimica et Cosmochimica Acta* **70**, 4507–4512.
41. Masbruch, M., Gardner, P.M., Nelson, N.C., Heilweil, V.M., Solder, J.E., Hess, M.D., McKinney, T.S., Briggs, M.A., Solomon, D.K., (2019) Evaluation of Groundwater Resources in the Spanish Valley Watershed, Grand and San Juan Counties, Utah. U.S. Geological Survey Scientific Investigations Report 2019-5062
42. McIntosh, J. C., & Ferguson, G. (2021). Deep meteoric water circulation in Earth's crust. *GRL*, **48**.
43. Murray, K. E., Reiners, P. W., Thomson, S. N., Robert, X., and Whipple, K. X. (2019) The thermochronologic record of erosion and magmatism in the Canyonlands region of the Colorado Plateau. *American Journal of Science* 319(5) 339-380.
44. Noyes C., Kim, J-H., Person, M., Ma, L., Fergurson, G., McIntosh, J.C (2021) Geochemical and Isotopic Assessment of hydraulic connectivity of a stacked aquifer system in the Lisbon Valley, Utah (USA), and critical evaluation of environmental tracers. Hydrogeology Journal.https://doi.org/10.1007/s10040-021-02361-9.
45. Nuccio V. F. and Condon S. M. (1996) Burial and Thermal History of the Paradox Basin, Utah and Colorado, and Petroleum Potential of the Middle Pennsylvanian Paradox Formation. *Evolution of Sedimentary Basins- Paradox Basin*. USGS Bulletin 2000-O.
46. Parry, W.T., Chan, M.A., Beitler, B. (2004) Chemical bleaching indicates episodes of fluid flow in deformation bands in sandstone. *AAPG Bulletin* **88**(2) 175-191
47. Porcelli D., Ballentine C. J. and Wieler R. (2002) An Overview of Noble Gas Geochemistry and Cosmochemistry.In: *Noble Gases in Geochemistry and Cosmochemistry.*(Eds: D. Porcelli, C.J. Ballentine,, R. Wieler) Reviews in Mineralogy and Geochemistry **47**. Geochemical Society, Mineralogical Society of America, Chapter 1, 1-19
48. Rønnevik C., Ksienzyk A. K., Fossen H. and Jacobs J. (2017) Thermal evolution and exhumation history of the Uncompahgre Plateau (northeastern Colorado Plateau), based on apatite fission track and (U-Th)-He thermochronology and zircon U-Pb dating. *Geosphere* **13**, 518–537.

49. Thackston J. W., McCulley B. L., and Preslo, L. M. (1981) Ground-water circulation in the western Paradox Basin, Utah: in Wiegand, D. L., ed., Geology of the Paradox basin: Rocky Mountain Association of Geologists Field Conference, p. 201-225
50. Torgersen T. (2010) Continental degassing flux of ^{4}He and its variability. *Geochemistry, Geophysics, Geosystems* **11**.
51. Torgersen T. (1980) Controls on pore-fluid concentration of ^{4}He and ^{222}Rn and the calculation of ^{4}He/^{222}Rn ages. *Journal of Geochemical Exploration* **13**, 57–75.
52. Torgersen T. (1989) Terrestrial helium degassing fluxes and the atmospheric helium budget: Implications with respect to the degassing processes of continental crust. *Chemical Geology: Isotope Geoscience section* **79**, 1–14.
53. Torgersen T. and Clarke W. B. (1985) Helium accumulation in groundwater, I: An evaluation of sources and the continental flux of crustal ^{4}He in the Great Artesian Basin, Australia. *Geochimica et Cosmochimica Acta* **49**, 1211–1218.
54. Trudgill B. D. (2011) Evolution of salt structures in the northern Paradox Basin: controls on evaporite deposition, salt wall growth and supra-salt stratigraphic architecture. *Basin Research* **23**, 208–238.
55. Tyne R. L., Barry P. H., Hillegonds D. J., Hunt A. G., Kulongoski J. T., Stephens M. J., Byrne D. J. and Ballentine C. J. (2019) A Novel Method for the Extraction, Purification, and Characterization of Noble Gases in Produced Fluids. *Geochemistry, Geophysics, Geosystems* 20, 5588–5597.
56. Tyne R. L., Barry P. H., Karolytė R., Byrne D. J., Kulongoski J. T., Hillegonds D. J. and Ballentine C. J. (2021) Investigating the effect of enhanced oil recovery on the noble gas signature of casing gases and produced waters from selected California oil fields. *Chemical Geology*
57. Wescott W. A. and Hood W. C. (1994) Hydrocarbon Generation and Migration Routes in the East Texas Basin1. *AAPG Bulletin* **78**, 287–306.
58. Young, E.D., Galy, A., Nagahara, H. (2002) Kinetic and equilibrium mass-dependent isotope fractionation laws in nature and their geochemical and cosmochemical significance *Geochimica et Cosmochimica Acta* **66**(6) 1095-1104.
59. Zhou Z. and Ballentine C. J. (2006) ^{4}He dating of groundwater associated with hydrocarbon reservoirs. *Chemical Geology* **226**, 309–327.

Supplementary only references

Battani A., Sarda P. and Prinzhofer A. (2000) Basin scale natural gas source, migration and trapping traced by noble gases and major elements: the Pakistan Indus basin. *Earth and Planetary Science Letters* **181**, 229–249.

Blackwell D. D. and Richards M. (2004) Geothermal map of North America. Geological Society of America.

Boving T. B. and Grathwohl P. (2001) Tracer diffusion coefficients in sedimentary rocks: correlation to porosity and hydraulic conductivity. *Journal of Contaminant Hydrology* **53**, 85–100.

Cater F. W. (1970) Geology of the Salt Anticline Region in Southwestern Colorado. US *Geological survey professional paper* **637**, Washington DC.

COGIS (2020). Production Data. Colorado oil and gas conservation commission. Department of Natural Resources. Available at: https://cogcc.state.co.us/data.html#/cogis. [Accessed November 2020]

Crovetto R., Fernández-Prini R. and Japas M. L. (1982) Solubilities of inert gases and methane in H_2O and in D_2O in the temperature range of 300 to 600 K. *Journal of Chemical Physics* **76**, 1077–1086.

DNR (2020). Production Data. Utah Division of oil, gas and mining. Department of Natural Resources. Available at: https://oilgas.ogm.utah.gov/oilgasweb/live-data-search/lds-prod/prod-lu.xhtml . [Accessed November 2020]

Fernández-Prini R., Alvarez J. L. and Harvey A. H. (2003) Henry's Constants and Vapor–Liquid Distribution Constants for Gaseous Solutes in H_2O and D_2O at High Temperatures. *Journal of Physical and Chemical Reference Data* **32**, 903–916.

Hendry, M.J., Barbour, S.L., Novakowski, K., Wassenaar, L.I., 2013. Paleohydrogeology of the Cretaceous sediments of the Williston Basin using stable isotopes of water. Water Resources Research 49, 4580-4592.

Mörner N.-A. and Etiope G. (2002) Carbon degassing from the lithosphere. *Global and Planetary Change* **33**, 185–203.

Ohsumi T. and Horibe Y. (1984) Diffusivity of He and Ar in deep-sea sediments. *Earth and Planetary Science Letters* **70**, 61–68.

Peng S., Hu Q. and Hamamoto S. (2012) Diffusivity of rocks: Gas diffusion measurements and correlation to porosity and pore size distribution. *Water Resources Research* **48**.

Pinti D. L., Wada N. and Matsuda J.I. (1999) Neon excess in pumice: volcanological implications. *Journal of Volcanology and Geothermal Research* **88**, 279–289.

Podosek F. A., Bernatowicz T. J. and Kramer F. E. (1981) Adsorption of xenon and krypton on shales. *Geochimica et Cosmochimica Acta* **45**, 2401–2415.

Podosek F. A., Honda M. and Ozima M. (1980) Sedimentary noble gases. *Geochimica et Cosmochimica Acta* **44**, 1875–1884.

Prinzhofer A., Vega M. A. G., Battani A. and Escudero M. (2000) Gas geochemistry of the Macuspana Basin (Mexico): thermogenic accumulations in sediments impregnated by bacterial gas. Marine and Petroleum Geology **17**, 1029–1040.

Purtschert R., Yokochi R., Jiang W., Lu Z.-T., Mueller P., Zappala J., Van Heerden E., Cason E., Lau M., Kieft T. L., Gerber C., Brennwald M. S. and Onstott T. C. (2021) Underground production of ^{81}Kr detected in subsurface fluids. *Geochimica et Cosmochimica Acta* **295**, 65–79.

Shackelford C. D. and Moore S. M. (2013) Fickian diffusion of radionuclides for engineered containment barriers: Diffusion coefficients, porosities, and complicating issues. *Engineering Geology* **152**, 133–147.

Smith S. P. and Kennedy B. M. (1983) The solubility of noble gases in water and in NaCl brine. *Geochimica et Cosmochimica Acta* **47**, 503–515.

Torgersen T. and Kennedy B. M. (1999) Air-Xe enrichments in Elk Hills oil field gases: role of water in migration and storage. Earth and Planetary Science Letters 167, 239–253.

Tripp B. (2010) Utah Potash: Resources, Production, and Exploration – Utah Geological Survey. Available at: https://geology.utah.gov/map-pub/survey-notes/utah-potash-resources-production-and-exploration/ [Accessed March 2021].

Turner C. E. and Fishman N. S. (1991) Jurassic Lake T'oo'dichi': A large alkaline, saline lake, Morrison Formation, eastern Colorado Plateau. *GSA Bulletin* **103**, 538–558.

Zhou Z., Ballentine C. J., Kipfer R., Schoell M. and Thibodeaux S. (2005) Noble gas tracing of groundwater/coalbed methane interaction in the San Juan Basin, USA. *Geochimica et Cosmochimica Acta* **69**, 5413–5428.